(2)

A Final Technical Report
Contract No. N00014-88-K-0111

# PLASTIC INSTABILITIES AND THEIR CONSEQUENCES IN STEELS AND OTHER HIGH STRENGTH ALLOYS



Submitted to:

Office of Naval Research
800 North Quincy Street
Arlington, Virginia 22217-5000

Attention: Dr. George R. Yoder
Scientific Officer
Materials Division
Code 1131



Submitted by:

Heinz G. F. Wilsdorf
William G. Reynolds Professor of Materials Science
[1/16/91-Professor Emeritus]

Report No. UVA/525425/MS91/101
September 1991

SCHOOL OF ENGINEERING AND
APPLIED SCIENCE

DEPARTMENT OF MATERIALS SCIENCE AND ENGINEERING



UNIVERSITY OF VIRGINIA
CHARLOTTESVILLE, VIRGINIA 22901

## UNIVERSITY OF VIRGINIA
### School of Engineering and Applied Science

The University of Virginia's School of Engineering and Applied Science has an undergraduate enrollment of approximately 1,500 students with a graduate enrollment of approximately 600. There are 160 faculty members, a majority of whom conduct research in addition to teaching.

Research is a vital part of the educational program and interests parallel academic specialties. These range from the classical engineering disciplines of Chemical, Civil, Electrical, and Mechanical and Aerospace to newer, more specialized fields of Applied Mechanics, Biomedical Engineering, Systems Engineering, Materials Science, Nuclear Engineering and Engineering Physics, Applied Mathematics and Computer Science. Within these disciplines there are well equipped laboratories for conducting highly specialized research. All departments offer the doctorate; Biomedical and Materials Science grant only graduate degrees. In addition, courses in the humanities are offered within the School.

The University of Virginia (which includes approximately 2,000 faculty and a total of full-time student enrollment of about 17,000), also offers professional degrees under the schools of Architecture, Law, Medicine, Nursing, Commerce, Business Administration, and Education. In addition, the College of Arts and Sciences houses departments of Mathematics, Physics, Chemistry and others relevant to the engineering research program. The School of Engineering and Applied Science is an integral part of this University community which provides opportunities for interdisciplinary work in pursuit of the basic goals of education, research, and public service.

A Final Technical Report
Contract No. N00014-88-K-0111

# PLASTIC INSTABILITIES AND THEIR CONSEQUENCES IN STEELS AND OTHER HIGH STRENGTH ALLOYS

Submitted to:

Office of Naval Research
800 North Quincy Street
Arlington, Virginia 22217-5000

Attention: Dr. George R. Yoder
Scientific Officer
Materials Division
Code 1131

Submitted by:

Heinz G. F. Wilsdorf
William G. Reynolds Professor of Materials Science
[1/16/91-Professor Emeritus]



Report No. UVA/525425/MS91/101
September 1991

Copy No. ____

# REPORT DOCUMENTATION PAGE

Form Approved
OMB No. 0704-0188



| 1. AGENCY USE ONLY (Leave blank) | 2. REPORT DATE | 3. REPORT TYPE AND DATES COVERED |
|---|---|---|
| | 09/01/91 | Final Technical Report 12/01/87 to 08/31/91 |

**4. TITLE AND SUBTITLE**

See 11.

**5. FUNDING NUMBERS**

N00014-88-K-0111

**6. AUTHOR(S)**

Heinz G. F. Wilsdorf

**7. PERFORMING ORGANIZATION NAME(S) AND ADDRESS(ES)**

University of Virginia
Department of Materials Science and Engineering
Thornton Hall
Charlottesville, VA 22903-2442

**8. PERFORMING ORGANIZATION REPORT NUMBER**

UVA/525425/MS91/101

**9. SPONSORING/MONITORING AGENCY NAME(S) AND ADDRESS(ES)**

Office of Naval Research Resident Representative
818 Connecticut Avenue
Eighth Floor
Washington, DC 20006

**10. SPONSORING/MONITORING AGENCY REPORT NUMBER**

**11. SUPPLEMENTARY NOTES**

The Investigation of the Fracture of Titanium Alloys
by in-situ and Analytical Microstructural Techniques

**12a. DISTRIBUTION/AVAILABILITY STATEMENT**

Approved for public release;
distribution unlimited

**12b. DISTRIBUTION CODE**

**13. ABSTRACT** (Maximum 200 words)

Some frequently used commercial high strength alloys have a tendency to fail catastrophically despite their ductile fracture mode. Apparently, these alloys develop instabilities during deformation which lead to local shear. The local shear areas often trigger catastrophic failure due to near adiabatic heating. An understanding of these phenomena was the object of the research reported here.

Ten high strength alloys have been studied as a function of strain rate. Specifically, the investigation of fracture surfaces of high strength 4340 steel samples tested in tension at quasi-static strain rates showed indeed localized melting accompanied by radial cracking. Surprisingly, at high strain rates up to $10^3$/s localized melting and radial cracking were absent; an analysis showed that this behavior was due to plastic deformation in the necked down cross-section which was heated above the ductile-brittle transition temperature range, then causing the alloy to fail in a fully ductile manner.

The temperature rise at the tip of a crack was modeled and calculated using defect deformation theory. The model predicted the correct temperature range in the process zone as well as a dependence on microstructure. The latter point was confirmed experimentally on Ti-6Al-4V tensile samples with three different microstructures. The interaction of dislocation cell walls with the spatially varying stress field of a moving crack was calculated and compared with high voltage electron microscope *in situ* observations.

| 14. SUBJECT TERMS | 15. NUMBER OF PAGES |
|---|---|
| | 80 |
| | 16. PRICE CODE |

| 17. SECURITY CLASSIFICATION OF REPORT | 18. SECURITY CLASSIFICATION OF THIS PAGE | 19. SECURITY CLASSIFICATION OF ABSTRACT | 20. LIMITATION OF ABSTRACT |
|---|---|---|---|
| Unclassified | | Unclassified | |

## FOREWORD

The experimental work on this contract has been carried out by Dr. David Makel who also supervised two undergraduate students, Robert Coneybeer and Steven Yu. He also was leading the research on the effect of microstructure on the temperature rise in the process zone in cooperation with Prof. D. Eylon, University of Dayton, Dayton, OH. Dr. K. Jagannadham, North Carolina State University, Raleigh, NC, contributed substantially to Section II,1 and II,3, and Prof. T. Pollock, Texas A&M University, College Station, TX to Section II,3. Day-to-day administration, correspondence, reports and manuscripts were promptly attended to by Ms. Paulette Hughes.

Very high strain rate experiments were carried out at the Fraunhofer-Institut für Angewandte Materialforschung, Bremen, Germany (Director Prof. Dr. H.-D. Kunze) by Dr. L. W. Meyer and Dipl. Ing. B. Reinders. The P.I. visited the Institut for one week in May 1988 and Dave Makel for one week in July 1991. These visits were sponsored by a travel grant from the NATO Scientific Affairs Division, Brussels, Belgium.

The frequent interaction on this research by Dr. George Yoder is very much appreciated.

PLASTIC INSTABILITIES AND THEIR CONSEQUENCES
IN STEELS AND OTHER HIGH STRENGTH ALLOYS

TABLE OF CONTENTS

## I. BACKGROUND AND RESEARCH OBJECTIVES.

During a study of microstructural fracture processes in titanium alloys it was discovered by stereo scanning electron microscopy (SEM) that some dimple walls were lined with small spheres and that the bottom of these dimples were covered with fine particles. These observations were made only in limited areas while the remaining fracture surface showed mostly the customary smooth dimples. It appeared that the melting point of these alloys had been exceeded at the final separation and that a small volume of molten volume had solidified very rapidly. Two explanations came immediately to mind: (i) a rapid temperature rise due to oxidation; (ii) a temperature rise caused by adiabatic, or near adiabatic shear. Both possibilities were carefully explored in two Ph.D. theses using Ti-8Mn (1) and Ti-10V-2Fe-3Al (2), respectively. The following results were obtained:

1. Tensile fracture in Argon yielded the same fracture surfaces with spheroidized dimple walls and "microroughness" as experiments in air. Thus, oxidation processes could not be the cause of the unusual surface features (1).
2. Temperatures reaching the melting point of titanium alloys should be visible as light. Exposures of photographic emulsions showed indeed light flashes at the location of fractures (1).
3. The microstructures immediately below the fracture surface were studied by a sectioning technique using the SEM. Evidence for localized high shear zones was found below spheroidized dimple surfaces (1).
4. Using finite element analysis (ANSYS) the dynamic interactions between stress, strain and temperature fields near a rapidly loaded crack tip were quantified for applied loading rates of up to $10^3$/s. Temperatures approaching 1,000°C were predicted for crack propagation speeds of 10 m/s and higher (2).
5. A preliminary computer model was used to calculate the temperature rise at a moving crack tip. Based on defect deformation theory, elements of the new model were loading rate, plastic work rate, dislocation density and velocity and plastic strain. The conditions under which the melting point of certain titanium alloys would be exceeded in small volume elements at the time of separation was predicted correctly (3).

The experimental results listed above were obtained by two independently

working investigators, on two different titanium alloys and at different fracture modes (plane stress for Ti-8Mn, plane strain for Ti10-2-3). In both cases the fractures were typically ductile exhibiting shear or necking and dimpled fracture surfaces. Also, it has to be pointed out that both alloys yielded at high stresses and that their heat conductivity was only 1/40 of copper.

There cannot be any doubt that the interpretation of a very high temperature rise at the crack tip was correct and that an exploration of the acting mechanism is needed from a scientific as well as from a practical point of view. The fractures under discussion are "catastrophic" and thus belong to one of the most undesirable classes of materials failures. Comparable fracture surface structures have been reported by other investigators on ballistic impact samples(4), and it stands to reason that an understanding of deformation heating at the crack tip could help to prevent catastrophic failures by avoiding the conditions leading to it.

The present research had specific objectives in answering the following questions: Are there materials characteristics, such as low heat conductivity, for example, that would be a prerequisite for catastrophic failure? How significant is the influence of metallurgical factors, such as grain size; or types, sites and distribution of precipites, for example? What are the preconditions for localized shear and near adiabatic or adiabatic shear? The thought that this type of fracture might occur also in steels is certainly very unsettling. Therefore, it was decided to investigate a 4340 steel and to study the effect of loading rate on its fracture mode. Secondly, during the first year of the contract period the results of a computer model* to predict the temperature rise at the crack tip of a fast crack became available (5) which indicated that the rate of dislocation generation was affecting the temperature rise more than the dislocation velocity. This was a clear indication that the microstructure was to have a significant influence on the deformation in the process zone of the crack tip. Based on our experience with titanium alloys, the effect of microstructure on localized melting in Ti-6Al-4V

---

*developed in cooperation with Dr. K. Jagannadham, N.C.S.U., Raleigh, N.C.

tensile samples was studied**(6). Since the processes taking place at the crack tip are extremely complex, more work had to be done on stress field variations and low energy dislocation substructures at a moving crack tip.

It was thought that a fuller understanding of the experimental results would be aided by a theoretical overview. For this reason we will begin our report with a description of a model for crack tip temperature rises which was completed at the beginning of the contract period(5).

**in cooperation with Dr. D. Eylon, University of Dayton, Dayton, OH.

II. RESULTS.

1. Model of the Temperature Rise at a Crack Tip.

(i) Approaches and Concepts.

Earlier attempts to predict a temperature increase at a moving crack tip have been based on continuum theory (7-9). These calculations have assumed the classical, ideal plastic zone in front of the crack and neglected to incorporate the plastic deformation preceding crack propagation. Also, materials parameters were assumed to be constant. Clearly, these approximations deteriorate at the high strain rates and temperatures seen by the tip.

The new model will attempt to arrive at the temperature in the process zone of a fast moving crack through calculations of the dissipation of deformational energy. Instead of using the integrated plastic work of the entire plastic zone, our model will use the dislocation density, $\rho$, in the much smaller process zone and the associated plastic work term.

A description of the energy terms related to the crack configuration will now be given. It is convenient to use a dislocation description of a continuous plastic crack, Fig. II,1-1. In view of the equilibrium of the crack configuration the

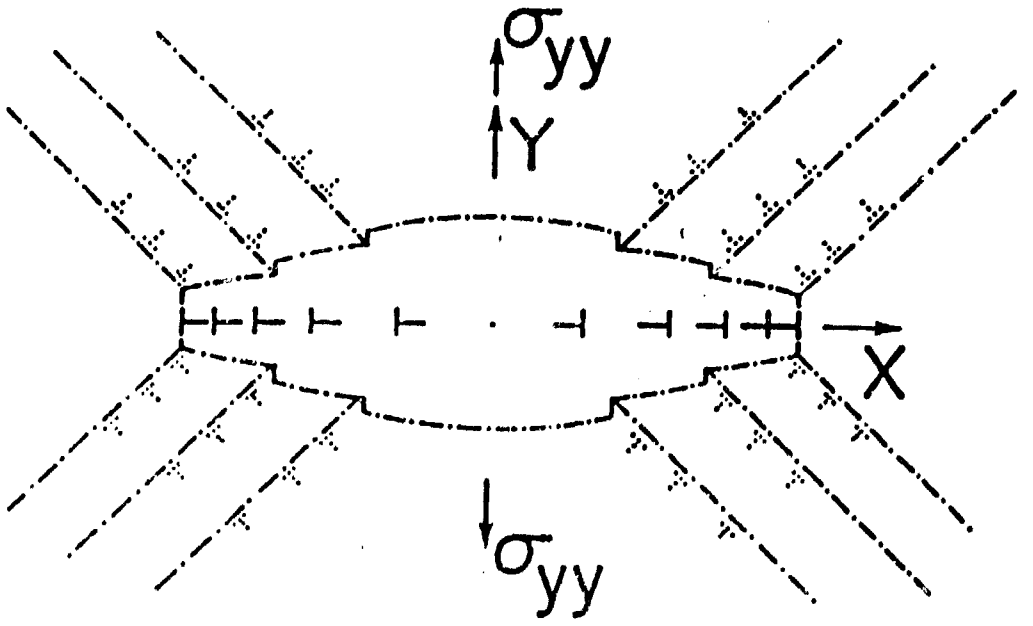


Fig. II,1-1. A continuous plastic crack represented by dislocations. Full symbols are crack dislocations. Dotted symbols are lattice dislocations.

following constitutive energy equations obtain (10).

$$E_{S_c} + E_{\ell_c} + E_{\ell_{c\ell}}/2 = E_{W_c}/2$$

$$E_{S_\ell} + E_{\ell_\ell} + E_{\ell_{c\ell}}/2 = -\left(E_f - E_{W_\ell}\right)/2 \qquad [1]$$

For an explanation of terms see Table I.

Then, the total energy of the crack configuration is

$$E_T = \left(E_\ell - E_{W_c} - E_{W_\ell} + E_f\right) + E_\gamma$$

$$= -\left(E_{W_c} + E_{W_\ell} - E_f\right)/2 + E_\gamma \qquad [2]$$

The elastic strain energy, $E_e$, includes the self energy and interaction energy of dislocations.

Table I

---

Description of Terms Used in Equations [1] and [2]

| | |
|---|---|
| $E_s$ | Self energy of dislocations |
| $E_\ell$ | Interaction energy of dislocations |
| $E_W$ | Work done by applied and crack tip stresses |
| $E_T$ | Total energy of crack configuration |
| $E_e$ | Elastic strain energy |
| $E_f$ | Lattice frictional stress |
| $E_\gamma$ | Term from newly created surface |

Subscript c stands for energy terms associated with crack dislocations, $\ell$ for lattice dislocations and $c\ell$ for the cross term between crack and lattice dislocations.

---

In all energy terms the velocity dependence for a fast moving plastic crack has

been incorporated as well as the modifications required for a dynamic crack (11).

The flow stress, $\sigma$, is related to plastic strain, $\varepsilon$, strain rate, $\dot{\varepsilon}$, and temperature, T, as

$$\sigma = \sigma\left(\varepsilon, \dot{\varepsilon}, T\right) \qquad [3]$$

and in differential form (12)

$$d\sigma = \left(\frac{\partial\sigma}{\partial\varepsilon}\right)_{\dot{\varepsilon},T} d\varepsilon + \left(\frac{\partial\sigma}{\partial\dot{\varepsilon}}\right)_{\varepsilon,T} d\dot{\varepsilon} + \left(\frac{\partial\sigma}{\partial T}\right)_{\varepsilon,\dot{\varepsilon}} dT \qquad [4]$$

When $\sigma$ reaches a maximum an instability occurs which will continue provided $d\sigma \leq 0$. Introducing shear stress, $\tau$, and shear strain, $\gamma$, for the case of an idealized shear band the stability relationship is

$$\left(\frac{d\tau}{d\gamma}\right) = \left(\frac{d\tau}{d\gamma}\right)_{\dot{\gamma},T} + \left(\frac{\partial\tau}{\partial\dot{\gamma}}\right)_{\gamma,T} \frac{d\dot{\gamma}}{d\gamma} + \left(\frac{\partial\tau}{\partial\gamma}\right)_{\gamma,\dot{\gamma}} \frac{dT}{d\gamma} = 0 \qquad [5]$$

The first term represents workhardening, the second the strain rate dependence of the shear stress, and the third term the thermal softening which is primarily responsible for the reduction of $\tau$ and therefore is negative.

The dislocation behavior in the process zone is governed by the following equations:

$$\sigma = \sigma_0 + \alpha G b \rho^{\frac{1}{2}} \qquad [6]$$

This workhardening equation is being observed in all metals and alloys. $\sigma_0$ is the lattice frictional stress, $\alpha$ a numerical factor of about 0.5, G is the shear modulus, b the Burgers vector and $\rho$ is the dislocation density.

Since the model should include high strain rate deformation, the relationship between $\rho$ and dislocation velocity, V, must be considered (13). The total mobile dislocation density, $\rho_m$, can be written as

$$\rho_m = \dot{\rho}\lambda = \dot{\rho} d / V \qquad [7]$$

With $\lambda$ the dislocation life time, $\dot{\rho}$ the dislocation generation rate and d the

distance moved by the dislocation, an expression for the strain rate can be set up

$$\dot{\varepsilon} = \rho d b \qquad [8]$$

Finally, a drag coefficient representing the heat producing forces has to be developed. The dissipating forces include phomons, electrons and thermoelastic losses, but assuming realistically that the dissipating viscous drag force predominates, the drag coefficient, B, can be written

$$B = \tau b / V \qquad [9]$$

Accounting for relativistic effects at high strain rates(14)

$$B = B_0 / \left(1 - V^2 / C_s^2\right)^{\frac{1}{2}} \qquad [10]$$

$B_0$ is the drag coefficient at rest and $C_s$ is the shear wave velocity. Now, the force required to overcome the viscous drag force by the dislocation can be written

$$F_{Drag} = \tau b = B_0 V / \left(1 - V^2 / C_s^2\right)^{\frac{1}{2}} \qquad [11]$$

The temperature dependence of $B_0$ is used in the following form (15-17)

$$B_0 = 3kT / 10 C_s b^2 \qquad [12]$$

where k is the Boltzmann constant.

(ii) Analysis of Changes in Various Quantities at the Crack Tip.

The improvements of the present model are not only due to employing decisive parameters of defect deformation theory applied to the processing zone at the crack tip, but can be realized only if the changes in front of the tip are incorporated for all critical quantities and thereby made an essential part of the computer calculations. The details of these considerations have been reported in ONR Technical Report UVA/525425/MS89/104 (August 1989). This report also contains the finite difference approximation of the heat equation used and the actual metallurgical data of alloy Ti-10-2-3. Further, and very importantly, it should be pointed out that the mechanical values used in the calculations are actual data taken from the doctoral research of J. D. Bryant (2). With the plastic

work dissipation rate, $\dot{W}$, written as follows

$$\dot{W} = \tau b \rho V = F_{Drag}\, \rho V = F_{Drag} \rho d / \Delta t \qquad [13]$$

a realistic energy dissipation accounting can be expected.

(iii) Results of Numerical Analysis.

Full details of all results obtained were provided in the ONR Technical Report cited above (19). Here, we will list the highlights which have a bearing on a fuller understanding of the theoretical and experimental results reported below. The first calculations determine the changes of eight quantities which will occur when the crack tip moves with velocity $V_c$. These quantities are:

(a) Stress field ahead of crack tip

(b) $\dot{\varepsilon}$ as function of lattice frictional stress

(c) Temperature (see Fig. II,1-2(a))

(d) Dislocation density

(e) Plastic work, $\dot{W}$, dissipated per unit time, t (see Fig. II-1-2(b))

(f) Increment of plastic strain

(g) Dislocation velocity

Most of the above are plotted as they change with distance from the crack tip.

After having determined the variations above, the maximum temperatures in the plastic zone were calculated for three different conditions of loading rate, $\dot{K}$, and crack velocity, $V_c$:

$\dot{K} = 680$ MPa / s, $V_c = 0.4$ m / s, $\beta = 10.0$
$\dot{K} = 888$ MPa / s, $V_c = 0.8$ m / s, $\beta = 20.0$
$\dot{K} = 1160$ MPa / s, $V_c = 1.6$ m / s, $\beta = 40.0$

$\beta$ is a parameter which is used for changing dislocation velocity as a function of applied stress. However, the direct influence of V was calculated too, and also the effect of the distance traveled by the dislocation which is, of course, of special importance for the high dislocation density in the process zone. In addition, the

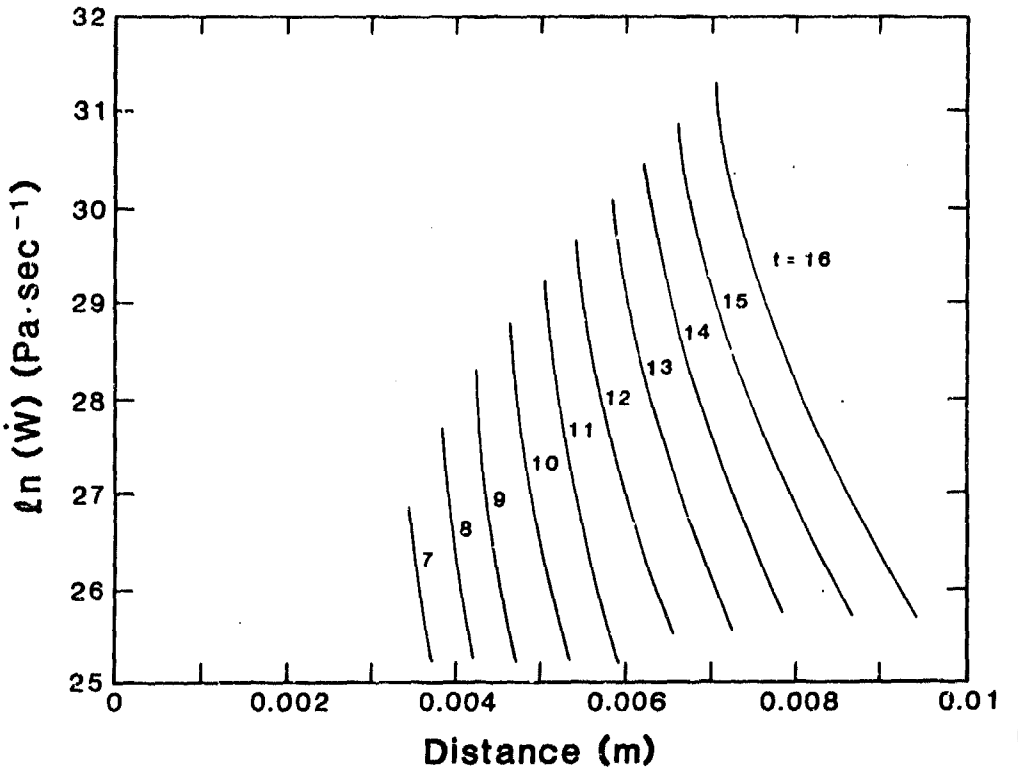


Fig. II,1-2. Results for calculations for loading rate $\dot{K}$ = 680 MPa/s and crack tip velocity $V_c$=0.4 m/s. Time units t=$10^{-4}$s. (a) Dissipated plastic work, $\dot{W}$, per unit time.

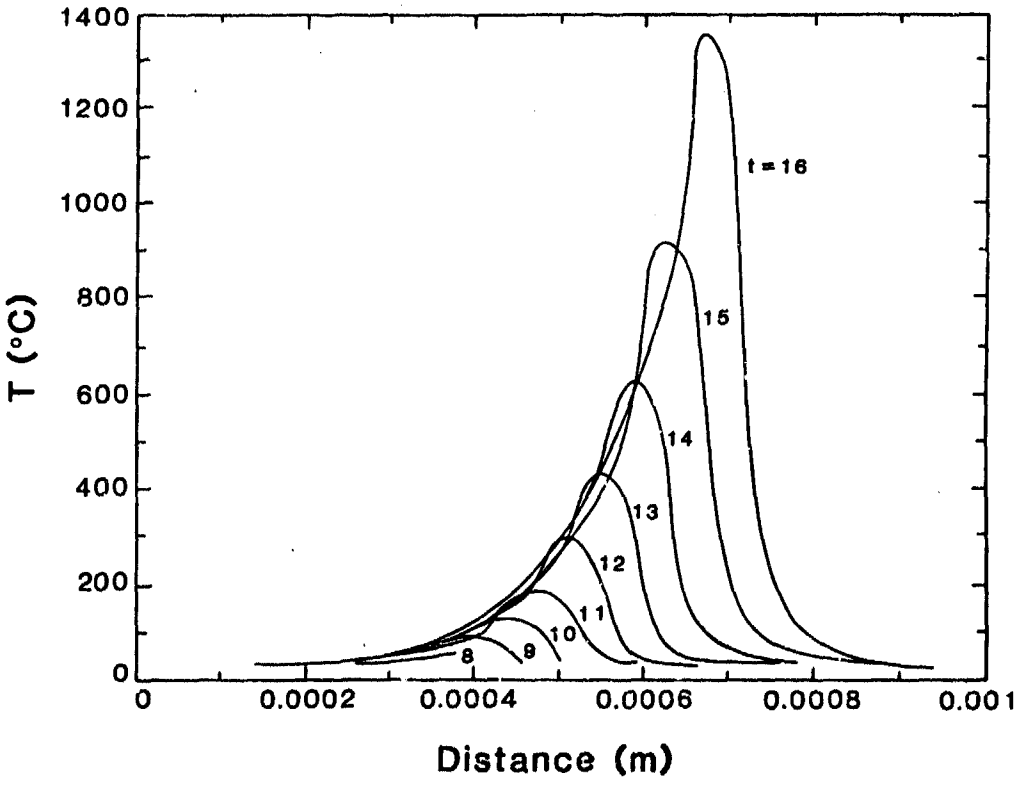


Fig. II,1-2. Results for calculations for loading rate $\dot{K}$ = 680 MPa/s and crack tip velocity $V_c$=0.4 m/s. Time units t=$10^{-4}$s. (b) Temperature ahead of crack tip as function of position from the start.

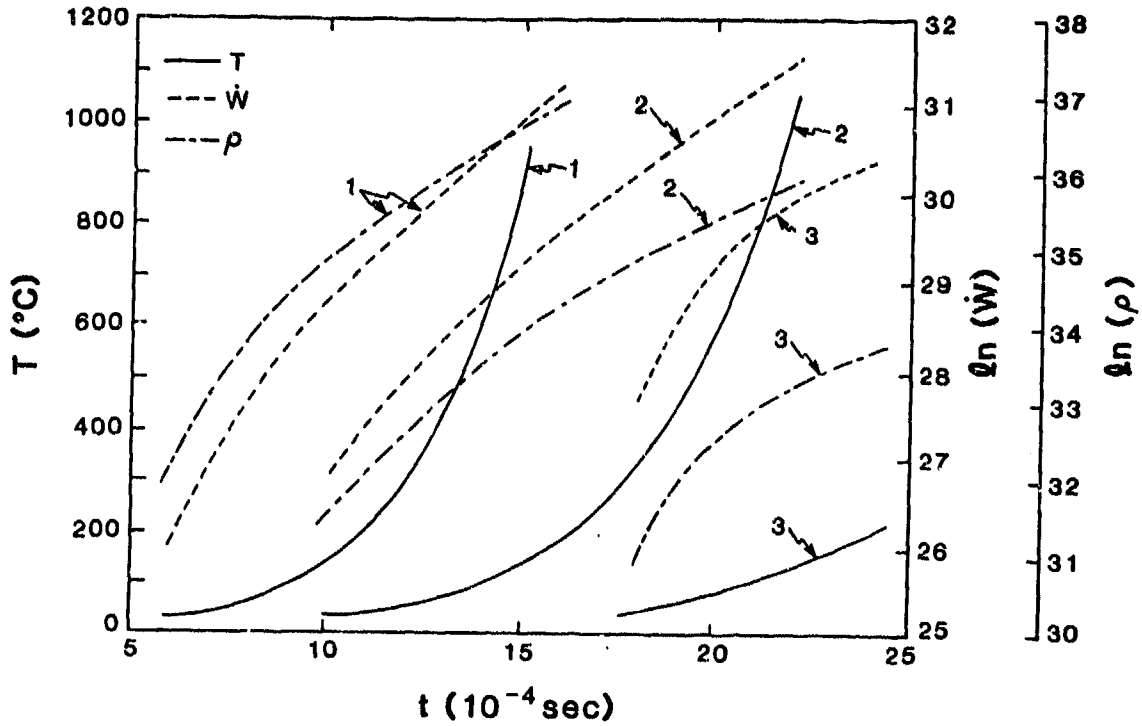


Fig. II,1-3. The maximum temperature attained in the plastic zone ahead of the crack tip, the rate of dissipation of plastic work, $\dot{W}$, and the dislocation density, shown as a function of loading time for three different conditions: (1) $\dot{K}$=680 MPa/s, $\sigma_0=\sigma_y/10$, $V_c$=0.4 m/s and $\beta$=10, (2) $\dot{K}$=888 MPa/s, $\sigma_0=\sigma_y/10$, $V_c$=0.8m/s and $\beta$=20, (3) $\dot{K}$=1160 MPa/s, $\sigma_0=\sigma_y/10$, $V_c$=1.6 m/s and $\beta$=40.

The value of $\beta$ has been increased by the same factor as that of $V_c$ so that the macroscopic strain rate is proportional to the loading rate.

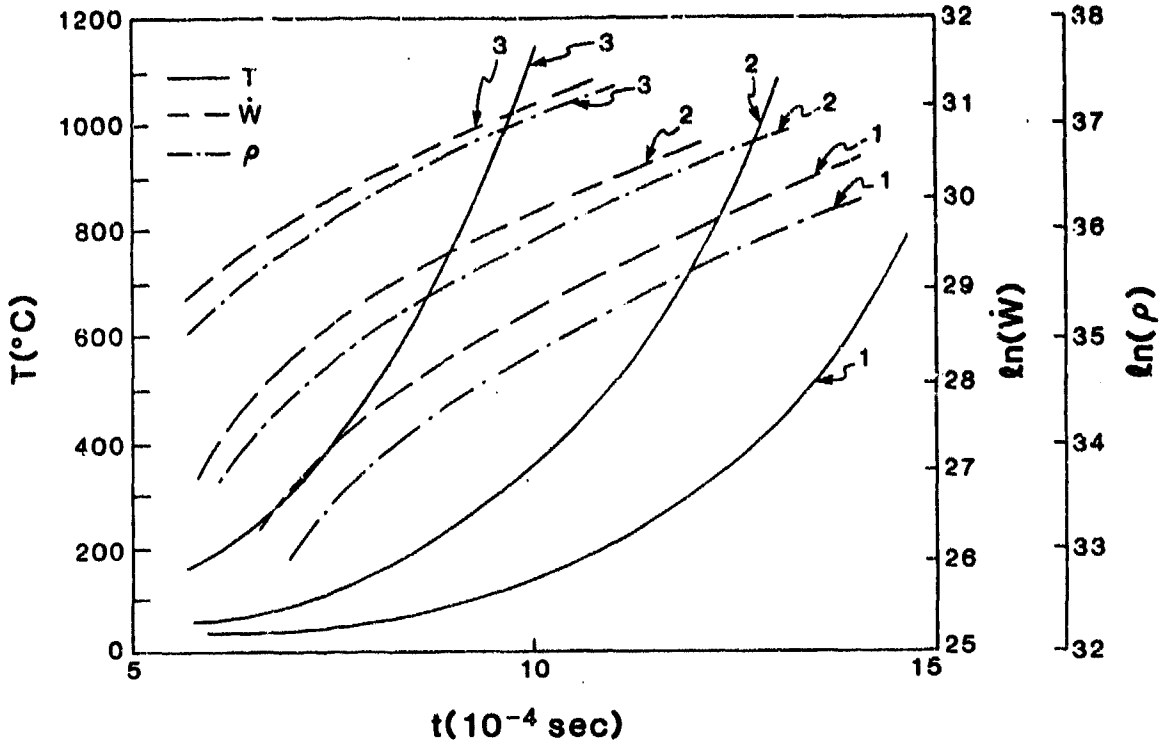


Fig. II,1-4. The maximum temperature attained in the plastic zone ahead of the crack tip, the rate of dissipation of plastic work, $\dot{W}$ and the dislocation density, $\rho$, shown as a function of loading time for three different conditions: (1) $\dot{K}$=680 MPa/s, $\sigma_0=\sigma_y/10$, $V_c$=0.4 m/s and $\beta$=10, (2) $\dot{K}$=888 MPa/s, $\sigma_0=\sigma_y/10$, $V_c$=0.8 m/s and $\beta$=10, (3) K=1160 MPa/s, $\sigma_0=\sigma_y/10$, $V_c$=1.6 m/s and $\beta$=10.

The value of $\beta$ has been kept constant for all values of the loading rate, $\dot{K}$, and crack tip velocity, $V_c$, so that the dislocation velocity and the strain rate near the crack tip are independent of the macroscopic strain rate.

effect of the crack tip radius on the temperature rise was determined. Two examples of the numerical analyses will be shown in Figs. II,1-3 and II,1-4. Please see the captions for details. Note that the temperatures often exceed 1,000°C.

(iv) Conclusions from Model Calculations

The energy changes associated with the fast propagation of elastic and plastic cracks have been modeled using crystal plasticity theory with special emphasis on the crack tip region. Dislocation generation rate and dislocation velocity were employed as key parameters in modeling the process zone within the classical plastic zone. The plastic work dissipated at the crack tip was found to result in very high temperature increases for high strength titanium alloys and the influence of the essential parameters on temperature was determined.

A number of general conclusions follow from the numerical results. It is assumed generally that higher loading rates and crack growth velocities will give rise to higher temperatures ahead of the crack tip. However, if the velocity of a very fast crack exceeds the rate of heat conduction the final temperature rise will be lower than that produced at a lower crack velocity. Similarly, a lower crack velocity for which the rate of dissipation of plastic work is low coupled with high thermal conductivity can also lead to low rates of temperature rise. We conclude that there exists a critical crack velocity as a function of thermal conductivity, and the rate of dissipation of plastic work in the process zone for which the build up of temperature becomes most efficient so that the highest temperature is attained. Increasing the crack tip velocity without raising the strain rate dependent lattice frictional stress can also lead to higher temperatures since the plastic zone will form more extensively. The microstructure associated with the region ahead of the crack tip process zone can alter these parameters. Changes in dislocation densities present in the process zone by an order of magnitude can alter the rate of increase of temperature in a given material for a given microstructure. Changing the microstructure can alter the dislocation density and the velocity leading to a different temperature change. The presence of obstacles to dislocation movement in the lattice reduces the dislocation velocity for the same crack tip velocity. In such materials, the frictional stress does not increase with increasing crack tip speed. We have found that the rate of increase of temperature is higher at higher crack growth rates provided the dislocation

velocity is kept constant. The model addressed temperature increases in the bulk only, but inter-void shear of ligaments which adds 300°C-500°C to the local total heat rise (20).

(v) Additional Heat Contribution.

The formation of dislocation cell walls has not been incorporated into the model. Together with second phase particles, cell walls can provide initiation sites for voids in the plastic zone. After void growth the final separation is completed by void coalescence. The latter process is taking place through shear of inter-void ligaments which, at that point, have a thickness of about one micrometer or less. The planar shape of the ligaments reduces the active glide systems to one or two (20) which opens up the possibility of adiabatic shear. For this to occur, an instability criterion is required that can be derived from equation [5]. It should be remembered that the reduction of shear stress, $\tau$, is due to the thermal softening term so that the instability can be written as follows

$$\left(\frac{d\tau}{d\gamma}\right)_T = -\left(\frac{\partial\tau}{\partial T}\right)_\gamma \frac{dT}{d\gamma} \qquad [14]$$

The critical shear that is a prerequisite for adiabatic shear can be calculated from

$$\gamma_{crit} = \frac{n\rho c}{\alpha(\partial\tau/\partial T)} \qquad [15]$$

where n is the workhardening exponent, c is the specific heat, and $\alpha$ a factor near unity. For a FCC metal $\gamma_{crit}$ was found to be about 4 (21). Assuming a dislocation to be the location of a linear heat source, Freudenthal and Weiner (47) calculated the temperature from the motion of dislocation groups in adiabatic shear. For our calculations a modified equation (21) was used

$$T = \frac{\tau VbN}{2\pi\kappa_L}\left(\frac{\pi\kappa}{LV}\right)^{\frac{1}{2}} \qquad [16]$$

N is the number of dislocations, $K_L$ is the heat conductivity, L is the distance of dislocation travel, and $\kappa=K_L$ divided by the density times the specific heat. Using for Ti-10-2-3 a shear stress of 190 MPa by estimating the bulk temperature to be

1,200°C and moving dislocation avalanches on glide planes 20 nm apart (corresponding to $\rho=10^{12}/cm^2$), one finds a temperature increase of 540°C.

(vi) Summary Statement.

Temperatures calculated from a deformation model of the process zone ahead of the crack tip can reach 1,200°C or more in localized areas. Shearing of intervoid ligaments during the final separation can add an additional 500°C. The sum of the two contributions exceeds the melting temperature of Ti-10-2-3 and explains the melting phenomenon observed by SEM stereo-microphotography in certain areas of the fracture surface.

The results obtained in this section made us realize that the microstructure had a much greater influence on the heating phenomenon than thought from the experimental results obtained originally from Ti-8Mn and Ti-10-2-3 both having quite different microstructures. Consequently, it was decided to investigate the influence of microstructure on local melting in another titanium alloy which permitted an accurate microstructural control by predesigned heat treatments (see section II,2). The development and consequences of low energy dislocation arrangements at the crack tip were also investigated (see section II,3). An extensive study was undertaken to understand the fracture behavior of a 4340 steel as a function of strain rate (see section II,4). In an appendix the coverage of molten fracture surface areas as a function of strain rate for Ti-10-2-3 will be reported.

2. The Influence of Microstructure on Heat Production in Ti-6-4***

(i) Introduction.

It follows from the previous section that the microstructure will affect heat production in the process zone. The present set of experiments was designed to

---

***This effort was a cooperation between Dr. David Makel, UVA, and Dr. D. Eylon, University of Dayton, Dayton, OH.

investigate the effect of Ti-6Al-4V microstructure on the formation of a number of features associated with localized melting. In particular, the possible role of common shear across α colony plates was considered in relation to the concentrated shear found below local heat-affected zones on the shear lip surfaces. The possible role of common dislocation glide paths across α-β interfaces within the α plate colonies on the initiation and development of larger scale localized and adiabatic shear in the shear lip region was of particular interest. These mechanisms are considered to play a critical role in the phenomenon of local surface melting at separation.

(ii) Experimental Investigation and Strength Data.

Tensile samples were cut from a 2.3-mm-thick mill-annealed sheet of commercial grade Ti-6Al-4V (Ti-6-4). The gage length of the samples was 15 mm, the width was 10.8 mm, and samples were cut with the final rolling direction parallel to the tensile axis.

The first samples were tested in the as-received mill-annealed condition. Two additional heat treatments were used to prepare the other samples. The first, designated heat-treatment A, was a β solutionizing for 2 hours at 1065°C, followed by furnace cooling to room temperature. This was aimed at developing α platelet structure of maximum α plate width and colony size. Heat-treatment B was a 4-hour soak at 927°C, below the β transus temperature, followed by furnace cooling to 700°C, at which point the samples were removed from the furnace and air cooled to room temperature. In contrast to heat-treatment A, this treatment produced large, low aspect ratio α grains separated by thin layers of β with some β at the triple point locations. Lack of a common glide path across the α-β interfaces in this microstructure was expected to cause a significant difference in the shear localization behavior and, hence, in the formation of the heat-affected areas.

Etched sections of the as-received mill-annealed sheet material are shown in Figure II,2-1. The microstructure consists of small (2 to 5μm) irregular α and β grains. At higher magnifications, the α grains appear slightly elongated parallel and perpendicular to the final rolling direction due to cross rolling. The microstructure of the heat-treatment A samples, shown in Figure II,2-2, consists of colonies of parallel α platelets which have an average diameter of about 73 μm, with the individual platelets having an average thickness of around 5 to 7μm,

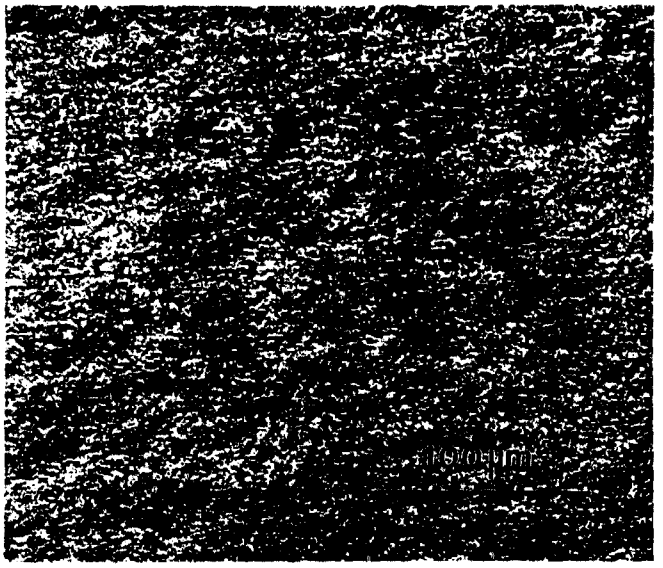

Fig. II,2-1. Etched sections of as-received mill-annealed material.

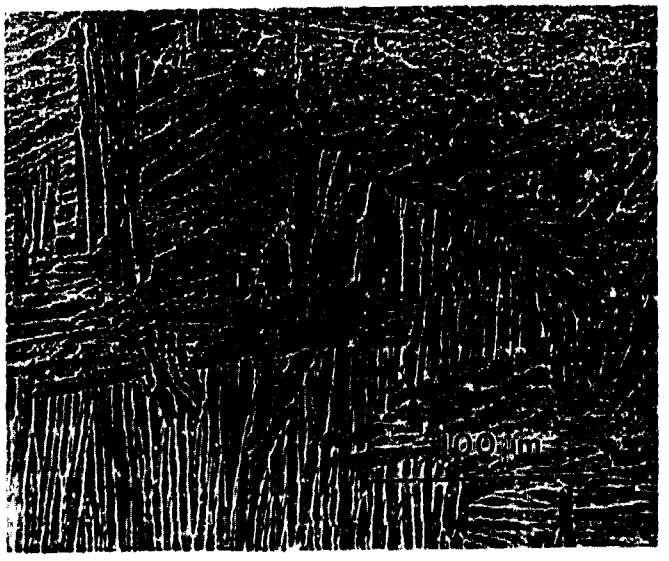

Fig. II,2-2. Etched sections of an α colony microstructure (heat-treatment A).

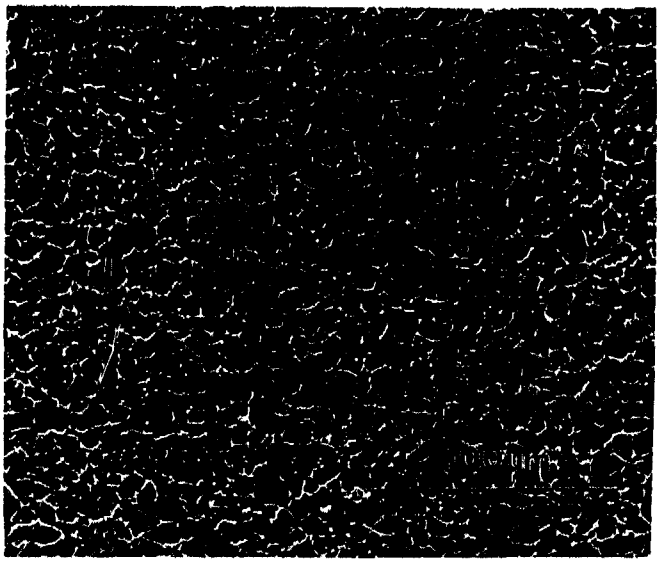

Fig. II,2-3. Etched sections of equiaxed α microstructure (heat-treatment B).

with an average aspect ratio of about 8:1. Heat-treatment B resulted in the microstructure shown in Figure II,2-3, which consists of coarse (10 to 20 μm), nearly equiaxed α particles separated by thin layers of β with some β also at triple point locations.

Results of the tensile tests are summarized in Table I. The colony microstructure samples (A) have a slightly higher ultimate tensile strength (UTS) than those with the equiaxed α(B) microstructure, and both of the heat treatments increased the UTS considerably over that of the mill-annealed samples.

TABLE I. Results of Tensile Tests (Average of Two Tests per Type)

| Heat Treatment | 0.2 Pct YS* | UTS** | Elongation (Pct) |
|---|---|---|---|
| As-received (mill annealed) | 809 MPa | 928 MPa | 32 |
| A ($\beta$ anneal + furnace cool) | 899 MPa | 991 MPa | 28 |
| B ($\alpha$-$\beta$ solutionize + furnace cool to 700°C/air cool) | 854 MPa | 972 MPa | 34 |
| Crosshead velocity | 0.05 cm/min | (5.5 X $10^{-4}s^{-1}$) | |

*YS=yield strength.

**UTS=ultimate tensile strength.

(iii) Fractographic Results

When viewed in a stereo microscope at magnifications of about 15 times, the fracture surfaces of the as-received and heat-treatment B samples can easily be separated into central crack areas lying generally perpendicular to the tensile axis and shear lip areas lying at angles of high shear (around 45 deg) to the tensile axis. Fracture surfaces of heat-treatment A samples do not contain clearly definable central crack areas, and the general surface is more irregular and tortuous, with most of the surfaces in high shear orientations. Differences in tortuosity between the two fracture surface types are obvious in regions of high shear, because the shear lips in the as-received and heat-treatment B samples are quite smooth over areas covering up to approximately one-half of the fracture surface.

From previous work, we know that there are four types of surface features associated with the formation of localized heat-affected regions (22,23): dimple-free open surface shear zones, shallow localized shear dimples, flat-topped

"transition" dimples, and spheroidized dimple walls and surface debris.**** Although all of these features are present in samples which contain areas of apparent localized melting, only the spheroidized dimple walls and surface debris represent locally melted material; the other surface features indicate the presence of localized shear, apparently a critical component in the melting at final separation but not necessarily an indication of a substantial local temperature increase.

An example of the heat-affected areas found in both the as-received and the heat-treatment B samples is shown in Figure II,2-4(a). This micrograph shows a dimple-free open surface shear zone directly above an area containing spheroidized dimple walls and surface debris. Below the area containing spheroidized material are flat-topped "transition" dimples, so named because they are considered to form during the transition between normal void growth to coalescence and void linkage by concentrated shear. An overview of the particular area shown in Figure II,2-4(a) is given in II,2-4(b). Here, one can see the open surface shear zone and heat-affected areas in the upper left corner (as indicated by the arrow). Moving down and to the right, one can see a continuous transition from heat-affected zone to transition dimples, to localized shear dimples, to the more common ductile dimples. This general positioning of the features of interest is typical of all of the heat-affected regions investigated to date.

By comparison, the fracture surfaces of the colony microstructures samples (A) are considerably different from the other microstructures, especially in the shear lip areas, which are much more angular and less ductile in appearance. An example of the angular shear lip areas of the colony samples isshown in Figure II,2-5(a). These surfaces consist of well-defined layers which, no doubt, are closely related to the colonies of $\alpha$ lamella in the microstructure.

Ductile dimples found on the surfaces of the as-received and the equiaxed $\alpha$ samples (B) generally range in size from about 1 to 5 μm in diameter. Dimples on the colony microstructure samples (A) fall into two general categories: those which have one particularly long axis apparently parallel to a long axis of the lamella and small dimples (about 0.2 to 2 μm in diameter). The presence of fine

---

****For full explanation of these terms see Appendix AI of this Report.

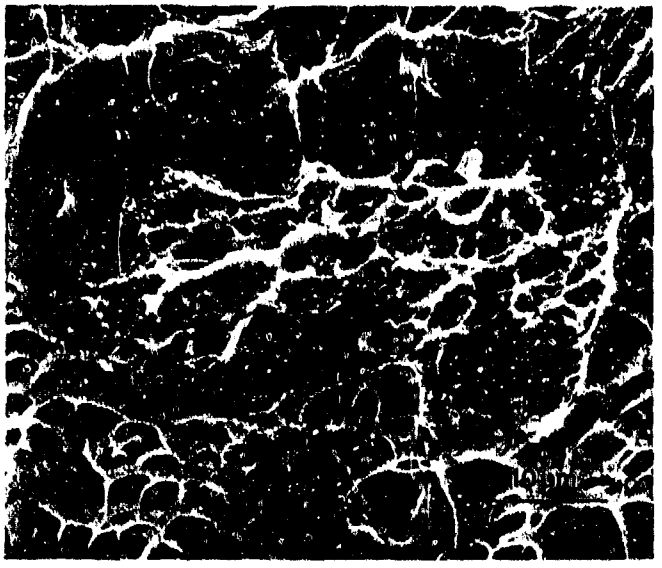

(*a*)

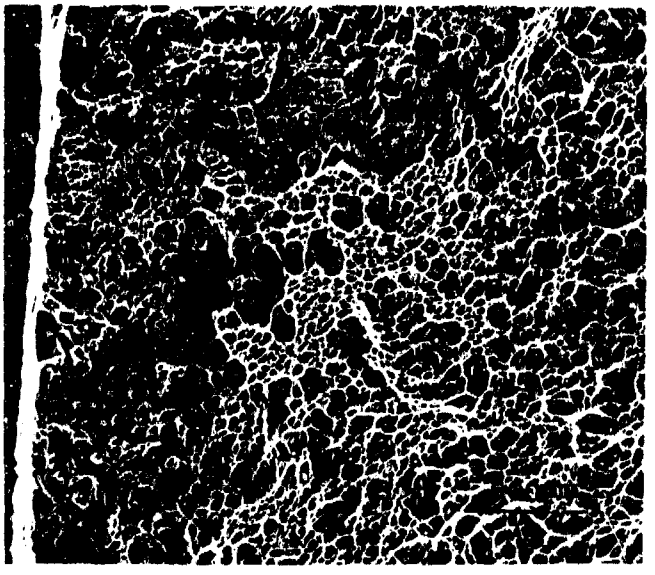

(*b*)

Fig. II,2-4. (a) Micrograph of equiaxed α (B) sample showing localized surface melting (center), an open surface shear zone (directly above melting), and transition dimples (bottom) and (b) lower magnification micrograph of the overall shear lip area containing the melted region shown in (a) (designated by the arrow in the upper left corner).

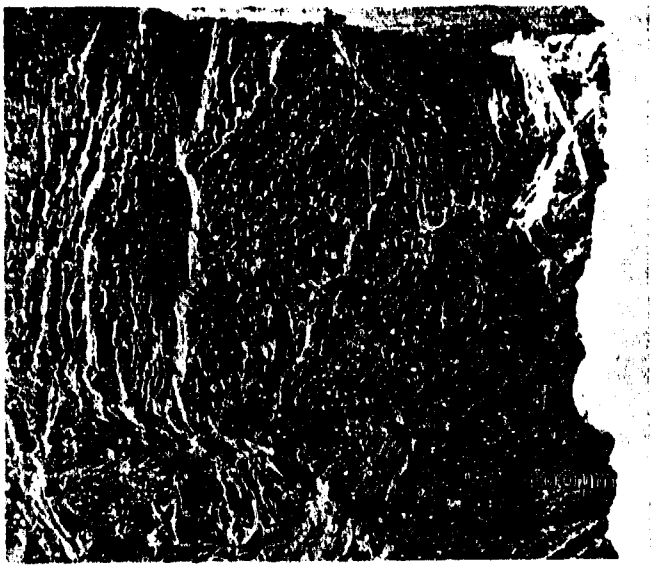

(*a*)

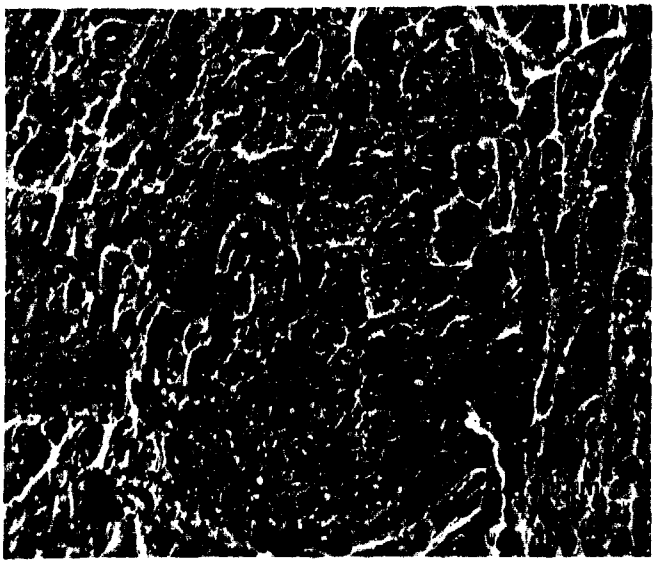

(*b*)

Fig. II,2-5. (a) Micrograph of the outer regions of the fracture surface of an α colony microstructure (A) sample and (b) higher magnification micrograph of the surface of an α colony microstructure (A) sample showing fine dimpling found on these surfaces.

dimples, as shown in Figure II,2-5(b), can be explained as a result of the constriction of the thickness of the volume involved in final separation by preferred separation along α-β interfaces.

The most important result of the microscopic examination of the fracture surfaces is that regions containing all of the surface features associated with high temperatures can be found on the as-received samples and the samples heat-treated to a coarse, equiaxed α microstructure (B), while there is a conspicuous absence of spheroidized dimple walls and surface debris on the colony microstructure samples (A) fracture surfaces. This indicates that the local melting phenomenon has been suppressed by varying the microstructure of the material.

(iv) Sectioning Results

The primary purpose of sectioning the samples was to observe the deformation below the fracture surface features of interest, in particular, localized shear deformation. Sections from the as-received samples contained little subsurface shear information, because the microstructure in these samples is extremely fine and the α grains are irregular in shape. For this reason, our investigations concentrated on comparing the sections of the coarse equiaxed α (B) and colony microstructure samples (A).

Subsurface deformation in the central crack regions of the equiaxed α samples show very little localized shear. This is to be expected since the central crack areas are essentially plane strain mode I regions. In the shear lip areas, however, subsurface shear is very apparent, as can be seen in Figure II,2-6, which shows a section below a shear lip area with arrows indicating some of the more obviously sheared β regions. Because of the irregular nature of the α particles, reliable measurements of shear are not possible, but the thickness of the shear zone under any particular surface appears to be generally between 1 and 5 μm.

In the heat-treatment A samples, the deflection of crack propagation direction by α colonies and α-β plate boundaries is obvious in many of the observed sections, an example of which is given in Figure II,2-7, as well as the preferred separation along prior β grain boundaries or colony boundaries, as demonstrated in Figure II,2-8. Figure II,2-9, which shows a subsurface secondary crack whose surface is made up of fine, coalesced ductile dimples, is an example of the

Fig. II,2-6. Section showing subsurface shear in an equiaxed α (B) sample (arrows indicate more obviously sheared β regions).

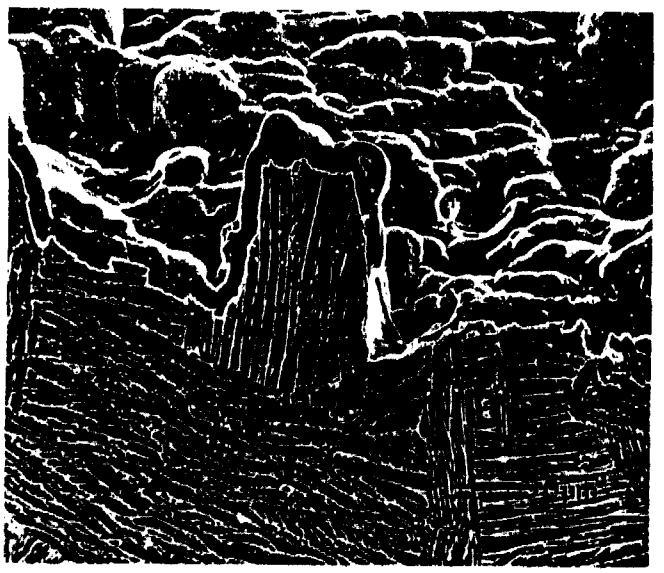

Fig. II,2-7. Section of an α colony microstructure (A) sample showing deflection of the crack path by an α colony.

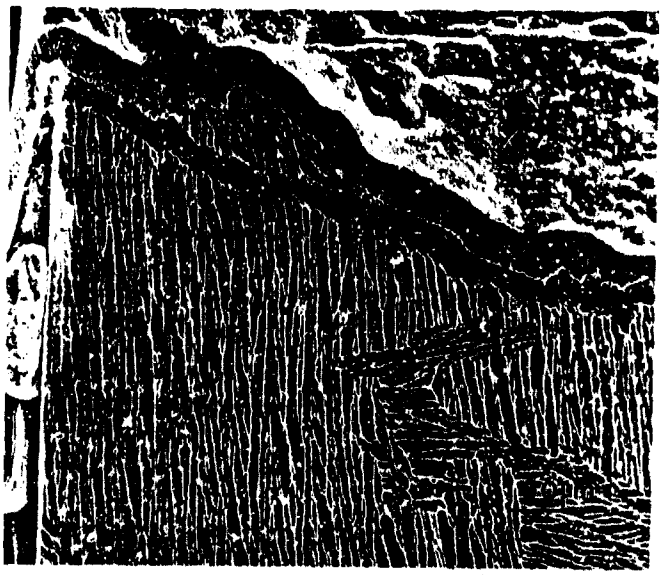

Fig. II,2-8. Section of an α colony microstructure (A) sample showing a crack path following a prior β grain boundary.

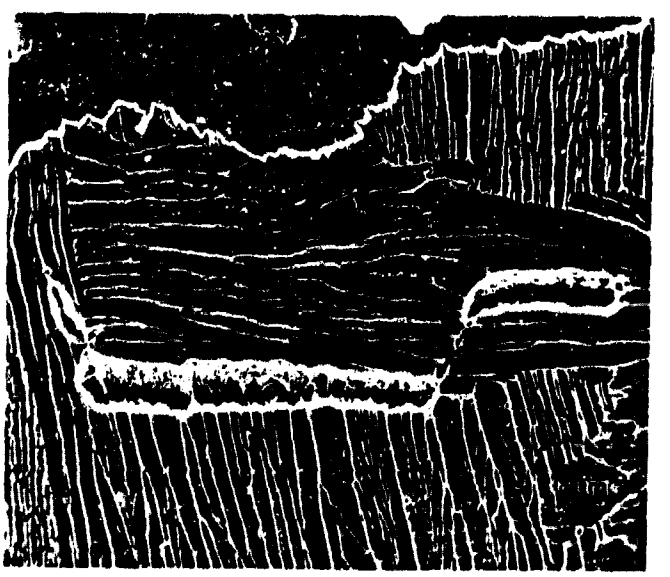

Fig. II,2-9. Section of an α colony microstructure sample showing a secondary crack with fine dimpling on the newly formed surfaces.

dimples which form along colony boundaries. These dimples are smaller as a result of a higher local void nucleation density along the boundary.

As to the localization of shear below the fracture of the colony samples (A), although some degree of localized shear can be seen in certain areas, the large-scale shear localization frequently found under the shear lip areas of the equiaxed α samples is absent in the colony samples. This is consistent with the lack of smooth shear area on the fracture surfaces.

In general, the deformation below the fracture surfaces indicates two major points of interest. First, the material below the shear lip regions showing localized melting is highly sheared parallel to the fracture surface. This large-scale localized shear is not found in the colony microstructure samples where the melting is essentially absent. Second, the colony microstructure samples show an increase in crack tortuosity due to crack deflection by the α colonies, prior β grain boundaries, and in some cases, individual α platelet boundaries.

(v) Conclusions.*****

1. Ti-6Al-4V tensile samples with microstructures of finely divided and equiaxed α particles (as-received and heat-treatment B) contain areas of localized melting near the outer edges of the fracture surface shear lips. Samples heat-treated to contain large colonies of α plates (heat-treatment A), however, show little or no signs of this local melting; *i.e.* , the localized surface melting effect can be suppressed by varying the microstructure of the material.
2. The material directly below the regions of localized melting displays highly concentrated shear. This concentrated shear is absent in the colony α samples, which show no signs of melting.
3. Fracture surfaces of the colony microstructure samples (A) have a much higher surface roughness and a lack of smooth shear regions compared to those of the other two microstructures tested.
4. Sections through the fracture surfaces show that prior β grain boundaries, individual α-β platelet interfaces, and colony boundaries

*****A full discussion of the experimental results can be found in the published work by D. Makel and D. Eylon (6).

all act as preferred separation surfaces in the α colony microstructure samples. Separation along these numerous internal boundaries explains the increased overall surface roughness of the α colony microstructure samples (A).

5. Fracture surfaces of α colony samples (A) contain regions of smaller, refined dimples and rows of elongated dimples not found in the mill-annealed or equiaxed α (B) samples. Dimple size refinement due to an increase in the void nucleation density may be a result of separation along the narrow interfaces found in the colony α samples, while the dimple elongation is most likely a result of separation across colonies of α lamella.
6. The mechanism suggested for the localized melting in the low aspect ratio α microstructure samples is a temperature rise through near adiabatic shear to a point below the β transus temperature followed by highly localized melting resulting from the heat generated during final inter-void ligament separation inside of the adiabatic shear bands.

3. Dislocation Cell Size Variations Caused by the Stress Field of a Moving Crack Tip.******

(i) Objectives.

As pointed out in section II,1 the dislocation generation rate, $\dot{\rho}$, at the crack tip and the dislocation velocity, V, have a significant influence on the

******In cooperation with K. Jagannadham, N.C.S.U., Raleigh, NC and T. C. Pollock, Texas A&M Univ., College Station, TX.

temperature rise. In this section another microstructural feature will be explored, namely dislocation cells. They form in the process zone as the predominant low energy dislocation arrangements and will affect $\dot{\rho}$ and V, in addition to promoting void initiation and crack propagation.

(ii) Theoretical Considerations and Calculations.

Calculating the interaction of a varying crack tip stress field with the dislocations in the process zone is a very demanding and complex task which has been published (29) and will not be repeated here. However, some highlights will be reported, in order to point out that this microstructural feature is part of any plastic crack moving through a ductile crystal. While the microstructure, described in section II,2 is controllable by heat treatments or compositional changes, the present study is researching an unavoidable problem common to all ductile fractures. It is particularly important if localized shear banding or near adiabatic shear are anticipated.

The spatially varying crack tip stress field is used to determine the dislocation density in the plastic zone. The rearrangement of dislocations is formulated using the minimization of the total energy of the configuration to form the cell structure in the presence of the spatially varying crack tip stress field. The equilibrium dislocation cell size is to be obtained for the lowest total energy of the configuration which consists of the self-energy and interaction energy terms associated with the dislocations within the cell walls and the work done by the crack tip stress field on the rearrangement of dislocations. A crack along (001) with two equally inclined {111} slip planes giving rise to a cell structure was analyzed. The results using the crack tip stress field to generate a plastic zone without general yield will illustrate that the cell size increases with increasing radial distance from the crack tip and increasing difference in the angular orientation from planes of maximum shear stress.

(iii) Results of Numerical Analysis

The cell size decreases as the crack tip is approached. Since the component of stress responsible for the glide force is largest near $\gamma=\pi/3$, the dislocation density for any given distance from the crack tip is also high, and, correspondingly, the cell size is small. The increase in cell size for larger

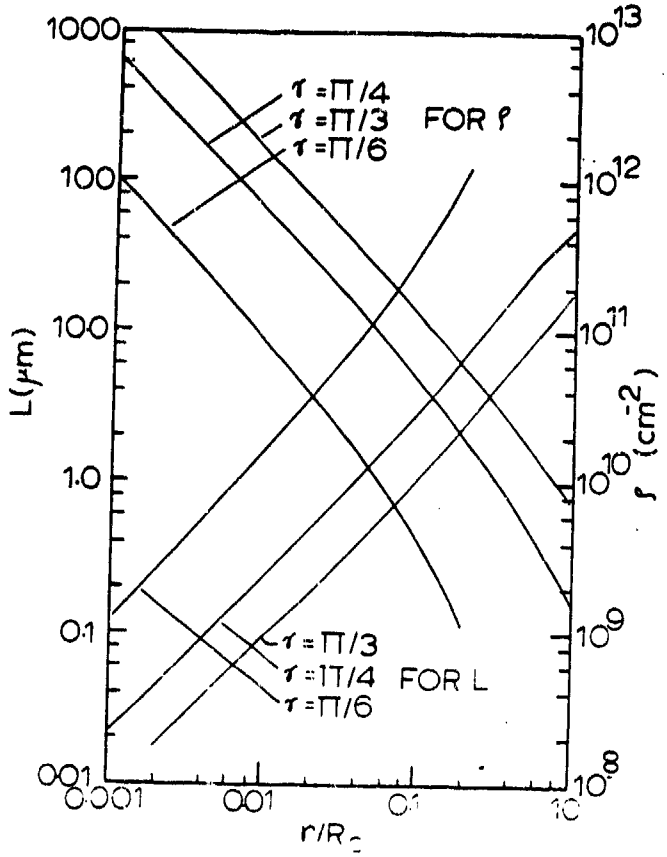


Fig. II,3-1. The variation of dislocation density and the cell size as a function of the distance from the crack tip for three values of the angular coordinate $\gamma$.

distances from the crack tip is an indication of the decrease in the crack tip stress field and the dislocation density. The work done by the crack tip stress field is a function of both the magnitude of the stress and the dislocation cell size. In order to lower the total energy or increase the negative term of work done by the stress, the cell size increases with decreasing dislocation density. However, the strain energy $U^*_{LR}$ of interaction of the stress field of the cell walls, which is a positive term, increases with increasing cell size so that the cell size cannot increase infinitely. Large sizes of cell structure are almost never reached except when the driving force for rearrangement of dislocations is present owing to a large energy gradient or when the mobility of dislocations is sufficiently high with low lattice frictional stress, for example under conditions of high temperature creep.

Whereas the formation of cell structures due to lowering of energy is a thermodynamic condition, the kinetics of attaining the stable cell structure is determined by the driving force for the rearrangement of dislocations. At smaller values of $\gamma$, such as $\pi/4$ or $\pi/6$, the stress component driving the dislocations into the cell walls decreases rapidly as a function of the distance from the crack tip, so that both a smaller dislocation density and a larger cell size are obtained, as shown in Fig. II,3-1. At larger distances from the crack tip, the dislocation density is sufficiently low that the large cell sizes obtained by the thermodynamical condition cannot be accommodated within the volume of the material. As a result, such large sizes of cell structure cannot be expected.

In the preceding analysis, the expressions for the stress field of an elastic crack have been used in the determination of the cell size. If the workhardening behavior of the material is taken into account such that a relation of the type

$$\sigma = \sigma_0 \varepsilon^n \qquad [17]$$

where $\sigma_0$ is a constant, n is the work-hardening exponent (10) and $\sigma$ is the flow stress of the material, the determination of the cell size requires further refinement. An incremental deformation model around the crack tip is useful to arrive at the dislocation substructure consisting of the cell walls. Specifically, the cell size is determined for a given level of applied stress wherein the plastic zone is developed. Thus, before the load is incremented in the analysis, the crack tip stress field is obtained at any position from the tip using equ. [17]. The strain $\varepsilon$ is given by $\rho bd$ where $d$ is the distance swept by the dislocations to form the cell walls. Subsequently, when the load is incremented, the elastic part of the crack configuration is determined in the presence of the stress field due to the cell walls within the plastic zone. Using the stress field of the new elastic part of the crack configuration, further minimization of the total energy to determine the cell size at any position from the tip is carried out in which the dislocation rearrange from the previous positions within the cell walls. Thus further shrinking of the cell walls under a higher level of stress field of the plastic crack can be incorporated into the analysis. In addition, crack growth can also be included in the analysis by changing the crack size between the increments of load, provided a decrease in the energy of the configuration is obtained.

(iv) Experimental Observations

It has been pointed out earlier that the formation of a dislocation cell structure is an important step in the crack growth. The orientation of the cell walls with respect to the crack depends very much on the operating slip planes present in the region ahead of the crack tip. In general, yielding occurs throughout the crystal before a crack is nucleated and further growth takes place in the already plastically deformed regions. Therefore it is difficult to distinguish the changes arising purely from the crack tip stress field. However, experimental observations on foils of sufficiently large thickness deformed *in situ* in the H.V. transmission electron microscope provide strong evidence for the formation of dislocation cell structures that are spatially dependent on the crack tip stress field.

This investigation technique is unique in that one can follow the emissions of dislocations from the crack tip together with dislocation distributions in the plastic zone, provided the tensile specimen is thick enough and a normal loading rate is being maintained. These points have been explored elsewhere (24-26). Straining thin crystals at very low strain rates has, in our opinion, yielded results in the past which have led to erroneous interpretations, such as the so-called "dislocation-free zone"; this concept was refuted very strongly (27). Therefore it is necessary to make use of thicker foils that are deformed continuously.

It has already been pointed out that dislocation densities in the plastic zone must be higher than those in the work-hardened crystal. The highest concentration occurs in the process zone where strain rates are higher by a factor of $10^2$ or $10^3$ compared with the strain rates in the plastic zone. The following investigations have been conducted to explore the dynamics of dislocation behavior and dislocation interaction ahead of the propagating crack tip with its stress field. This involves very large numbers of dislocations and the corresponding low energy dislocation configurations to be formed ahead of the crack tip.

Experiments were conducted with high purity, seven-pass beryllium single crystals cut parallel to the basal plane. Straining in directions lying in the (0001) plane resulted in plastic deformation on glide planes belonging to the prism system (28). The dislocation cell structure which developed during deformation was relatively large (28) and permitted a clear picture at 500 kV from specimens 4-5 μm thick. A sequence of three micrographs taken from a propagating crack

will be evaluated in the light of our analytical results.

These micrographs illustrate the nature of interaction of the crack tip with dislocations and their assemblies. Figure II,3-2a shows a crack tip with a sharp point which had opened to a width of 0.6 μm. It stopped at the branching point of two strong cell walls. Figure II,3-2b shows the same crack after a strain increment. The crack had moved approximately 1.2 μm and again stopped at a branching point. The directional deviation was 30° to the right from the crack in Fig. II,3-2a. A further strain increment caused the narrow crack to move 2.5 μm and to open up a to a width of almost 0.9 μm. The directional change was 25° to the left, *i.e.* the crack was now nearly parallel to the direction it had before the two strain increments.

As had been expected from the theoretical treatment above, substantial changes in the dislocation density and the dislocation arrangement took place ahead of the crack tip. Some of the significant changes will be pointed out with the help of the drawings in Figs. 13a-13c. The sketches serve to direct the reader to follow the major changes and therefore show only the highlights of the corresponding micrographs. A general comment regarding the visible dislocation cell walls seems to be in order.

In view of the theoretical treatment presented in this paper, our first attention should be given to a "fan" of dislocation walls in Fig. II,3-2a which almost blends into the background. This fan-shaped area is marked "SB" in Fig. II,3-3a and is located towards the left of the tip, filling the better part of the center to a distance of about 2 μm. This dislocation arrangement exists only where cell walls are absent. An even clearer indication of the presence of dislocation patterns in an arrangement following the stress field lines of the crack is seen in Fig. II,3-2b. Again the "fan" is located in a dislocation cell-free area and extends approximately 2 μm.

In order to facilitate the orientation of significant features affected by the stress fields of the three crack tips, we wish to point out three areas marked in Figs. II,13a-13c. Areas A and B are both visible in Figs. II,3-3a and II,3-3b, and B is still partly to be seen in Fig. II,3-3c. Area D is not yet established in Fig. II,3-3a but appears in Fig. II,3-3b and is the significant reference point for Fig. II,3-3c.

A comparison between Figs. II,3-2a and II,3-2b allows the conclusion that the crack has followed the dislocation boundary (DB) number 1 and disappeared

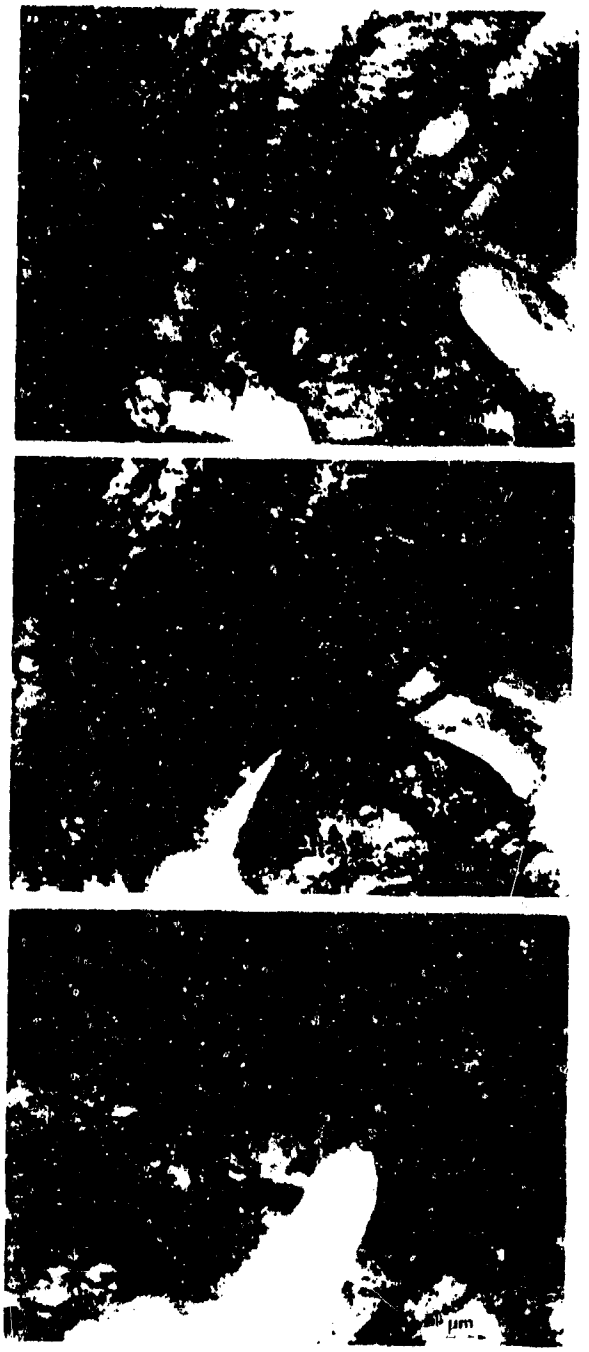


Fig. II,3-2. Sequence of a propagating crack in a foil of beryllium produced by *in situ* straining in a 500 kV electron microscope: (a) first position after stopping the straining device; (b) position of crack after first strain increment (distance of crack advance is 1.2 μm); (c) a further strain increment moved the crack approximately 2.5 μm.

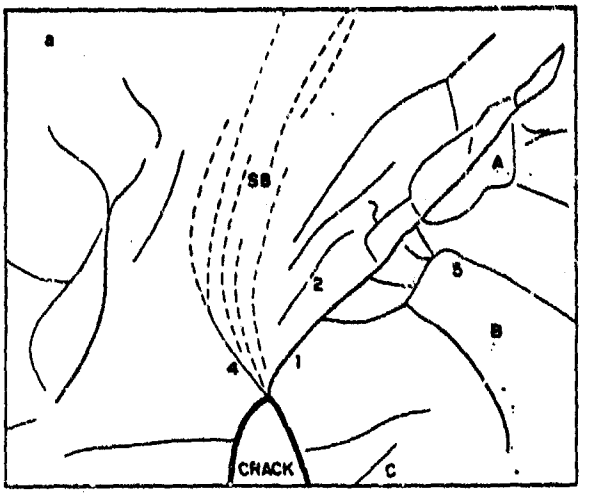


(a)

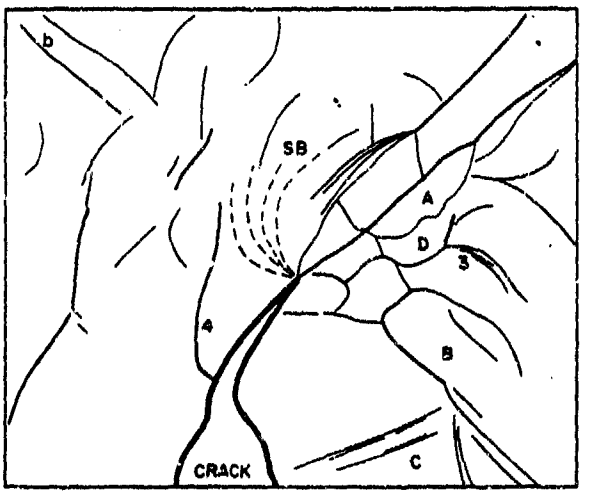


(b)

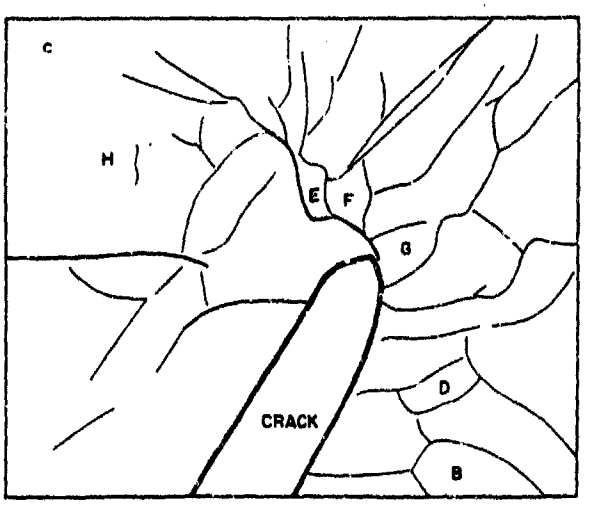


(c)

Fig. II,3-3. Drawings made from photographic negatives to highlight dislocation cell wall changes which occurred during crack propagation. The dashed lines in (a) and (b) indicate dislocation assemblies which follow crack tip stress field contour lines.

together with neighboring DB number 2 up to the stopping point. A new DB number 3 appeared on the right well ahead of the advancing crack (Fig. 12b). DB number 4 in Fig. II,3-2b is the only part remaining from the original number 4 which was forming the V at the branching point in Fig. II,3-2a; the "fan" SB in the same micrographs virtually disappeared and apparently was incorporated in other cell walls, as seen by the muddled contrast between perpendicular cell walls, *i.e.* dark lines, caused by cell walls which are inclined against the beam direction. It is also useful to note that the area B is smaller after the crack has progressed and that DB number 5 as part of this cell has moved 0.5 μm to the right.

As indicated above, area D is the most significant reference mark in Fig. II,3-2c in order to relate the newly formed part of the crack after the second strain increment. The width of the crack has increased from 0.2 to 0.8 μm and the tip is now perfectly blunted. Figure II,3-2c lends itself to comparison between the sizes of cells as projected into the image plane. While the cells to the right of the crack in Fig. II,3-2c were developed by the earlier crack propagation, the large cells to the left appear to be representative of the cell sizes in the work-hardened crystal before the crack moved in. Three cells (E, F and G) cover areas of 0.1, 0.25 and 0.375 $\mu m^2$. The open areas to the left cover 4 $\mu^2$ and between 2 and 1 $\mu^2$. The observations made in this section will now be evaluated in the light of the theoretical predictions.

During the past few decades, theoretical research predicted that dislocations should be emitted from crack tips and that crack tip stress fields should be interacting with dislocations. Experimental results to verify these concepts are not so plentiful. The three micrographs shown in Fig. II,3-2 provide evidence that indeed large numbers of glide dislocations are emitted from the tips. This can be seen (i) by comparing the number and the size of dislocation cells with those in volume elements outside of the crack tip stress field, and (ii) by the presence of dislocation "fans" tracing a significant part of the crack tip stress field. One can estimate that the dislocation density ahead of the crack tip is one to two orders magnitude higher than in the surrounding volume.

Furthermore, it is possible to deduce from this sequence the dynamics of the crack tip interactions with the defect structure into which the crack is moving. The most obvious evidence is to be found in following the changes that

have been imposed on the cell walls, which can move distances of at least 0.5 μm; they can expand and/or contract; they can be newly created and/or dissipated; and they can be changed in strength, *i.e.* dislocation content. The result is not only a continuous or discontinuous change in dislocation density, but at the same time a change in misorientation with which the crack tip stress field will have to interact.

The lowering of energy in the system served as a natural selection process for local occurrences. For example, the emission of dislocations is reduced when a crack propagates along a cell wall (Fig. II,3-2b). The principle governing this process has been elaborated on in an earlier paper (30), but it is seen immediately that the attraction of wall dislocations into the crack surface amounts to a drastic lowering of the system's energy and this will of course facilitate the propagation of the crack. That indeed there was a reduction in dislocation emission can be seen from the narrow width of the crack (Fig. II,3-2b) when compared with the ductile crack in Fig. II,3-2c. The movement of the crack along such boundaries results in the fracture surface morphology that may be easily confused with brittle cleavage. It is clear, however, that this movement cannot happen without previous plastic strain, which resulted in the formation of the cell boundary. The crack tip area will undoubtedly provide the most important sources for glide dislocations in the propagation of ductile cracks. However, additional positive and negative sources will be activated in the area ahead of the tip. It is interesting to note that the path of the crack pictured in Fig. II,3-2c went through the volume of the "fan" SB in Fig. II,3-2b which represented an area of high dislocation density.

(v) Summary and conclusions

The formation of a cell structure in the region of the plastic zone ahead of a crack tip is determined by minimizing the total energy of the configuration. The work done by the spatially varying crack tip stress field on the rearrangement of dislocations into cell walls is used to determine the variation of cell size in the plastic zone. A (001) crack with two equally inclined {111} slip planes containing dislocations with $(a/2)[101]$-type Burgers' vectors is used to analyze the variation of cell sizes in aluminum. It is found that the cell size increases with increasing distance from the crack tip and as the angular coordinate from the crack plane increasingly differs from 60°. These results are consistent with the experimentally observed variation of cell size in the plastic zone. Electron

microscopic observations of dislocation cell walls formed in the region ahead of the crack tip in thick foils of beryllium deformed *in situ* the tensile stage of a high voltage electron microscope illustrate the influence of the crack tip stress field on the formation of the dislocation cell structure. The "fan"-shaped dislocation cell walls and the rearrangement of dislocation cell walls during each stage of crack growth point to the validity of the ideas associated with the formation of low energy dislocation structures in the region ahead of the crack tip. They are of great importance for all ductile fractures, specifically for crack propagation and void initiation in the process zones.

4. Localized Melting at the Separation of AISI 4340 Steel Tensile Samples.

(i) Introduction

High strength alloys are known to fail catastrophically due to instabilities which often lead to strain localization. Work in the past was done on alloys having very low heat conductivity (1,2,31). The question whether the localized melting at separation is indeed a general phenomenon is going to be studied in a high strength steel, i.e. AISI 4340. Specifically, the effects of strain rate and of increased stored elastic energy on separation were to be documented. The fracture mechanisms operating were to be deduced by SEM stereo fractography. The theoretical analyses worked out earlier (21,5,31) will be applied.

(ii) Experimental Procedure.

The material used in the present study was AISI 4340 ultrahigh strength steel. Cylindrical tensile samples with a gage diameter of 3.4 mm and a gage length of 10 mm were machined with the tensile axis parallel to the final rolling direction. Heat treatment of the samples started with a one hour austenitizing in sealed quartz capsules filled with argon, after which the capsules were broken and the samples quenched into stirred oil. Tempering was done at 435°C in a tube furnace purged with argon, after which the samples were air cooled in the argon

purged tube.

Three types of tensile tests were conducted, normal quasi-static tests with an applied strain rate of $8.3 \times 10^{-1}$ $sec^{-1}$, high rate tests conducted at the Fraunhofer Institute in Bremen, Germany at rates between 83 $sec^{-1}$ and 3000 $sec^{-1}$ using a flywheel device, and ultra-soft tests, which were similar to the quasi-static tests except that a large spring was placed between the crosshead of the testing machine and the sample, reducing the stiffness of the test system from about $2.5 \times 10^{7}$ N/m to approximately $4.8 \times 10^{4}$ N/m. The ultra-soft tests were designed to study the effect of increased stored elastic energy on separation.

A profile projector was used to make 100X tracings of both pieces of the post-fractured tensile samples. These tracings could then be used to "reconstruct" the shape of the samples just prior to separation. This facilitated the estimation of the volumes included in the sample necks.

(iii) Experimental Results

Tensile Results

The quasi-static mechanical properties of the samples are summarized in Table II. These results agree with previous results of AISI 4340 heat treated to a 435°temper(32). High rate tests performed at the Fraunhofer Institute in Bremen, Germany show a slight increase in UTS and yield strength with increasing rate, but elastic wave effects make these results difficult to interpret. Non-linearities in the elastic portion of the load-elongation curve introduced by the large spring used in the ultra-soft device make yield stress and elongation determinations difficult, but the measured UTS values agree with that of the quasi-static tests.

TABLE II. Quasi-Static Tensile Results
(average of two tests)

| AISI 4340 Steel (435°C temper) |
|---|
| Ultimate Tensile Stress: 1320 MPa |
| 0.2% Offset Yield Stress: 1230 MPa |
| Elongation at UTS: 1.02 mm |
| Elongation at Fracture: 2.25 mm |

Fracture surface features which have been associated with localized melting at separation in titanium alloy tensile samples are shown in Figure II,4-1a and defined in Figure II,4-1b. These unusual fracture surface features fall into three general categories, "open surface shear zones," "transition dimples," and mixed mode spheroidized dimples with associated spheroidized surface debris. All of these features are found in areas of shear, typically in the shear lip, and the surfaces of the melted regions and transition dimples are finely textured, a feature called "microroughening."

Sections cut through the locally melted regions accentuate the role of shear in the melting process. Highly localized shear is found directly below the melted regions, as shown in Figure II,4-2 for Ti8Mn heat treated to an acicular alpha platelet microstructure.

At magnifications of 24X the fracture surfaces of the normal quasi-static steel test samples, as shown in Figure II,4-3a contain three distinct regions; a central fibrous area surrounded by an annulus of radial cracking and an outer annulus of shear lip. Fracture surfaces of the high rate and ultra-soft tests, examples of which are shown in Figures II,4-3b and II,4-3c respectively, contain only central fibrous central cracking areas surrounded by shear lip. The absence of radial cracking is an important feature which will be discussed later.

All steel fracture surfaces were carefully inspected at higher magnifications for indications of localized melting. The first samples investigated were those from the high rate tests and these surfaces showed no signs of melting to the resolution limit of the microscope (approx. 60 Å). Likewise, the ultra-soft test samples showed no signs of melting and the surfaces were generally indistinguishable from those of the high rate tests.

Surfaces resulting from the normal quasi-static tests were considerably different. At numerous points to the outside of the shear lip areas these surfaces contained regions which were similar to locally melted regions found in the earlier titanium studies. Figure II,4-4a shows a shear lip of one of the normal quasi-static test samples with the box indicating the position of the area shown in Figure II,4-4b. Figure II,4-4b contains three locally melted areas, one of which is shown at higher magnification in Figure II,4-4c. The regions of melting in the steel samples are in some ways different from those in titanium, as shown in Figure II,4-1, but they bear important similarities.

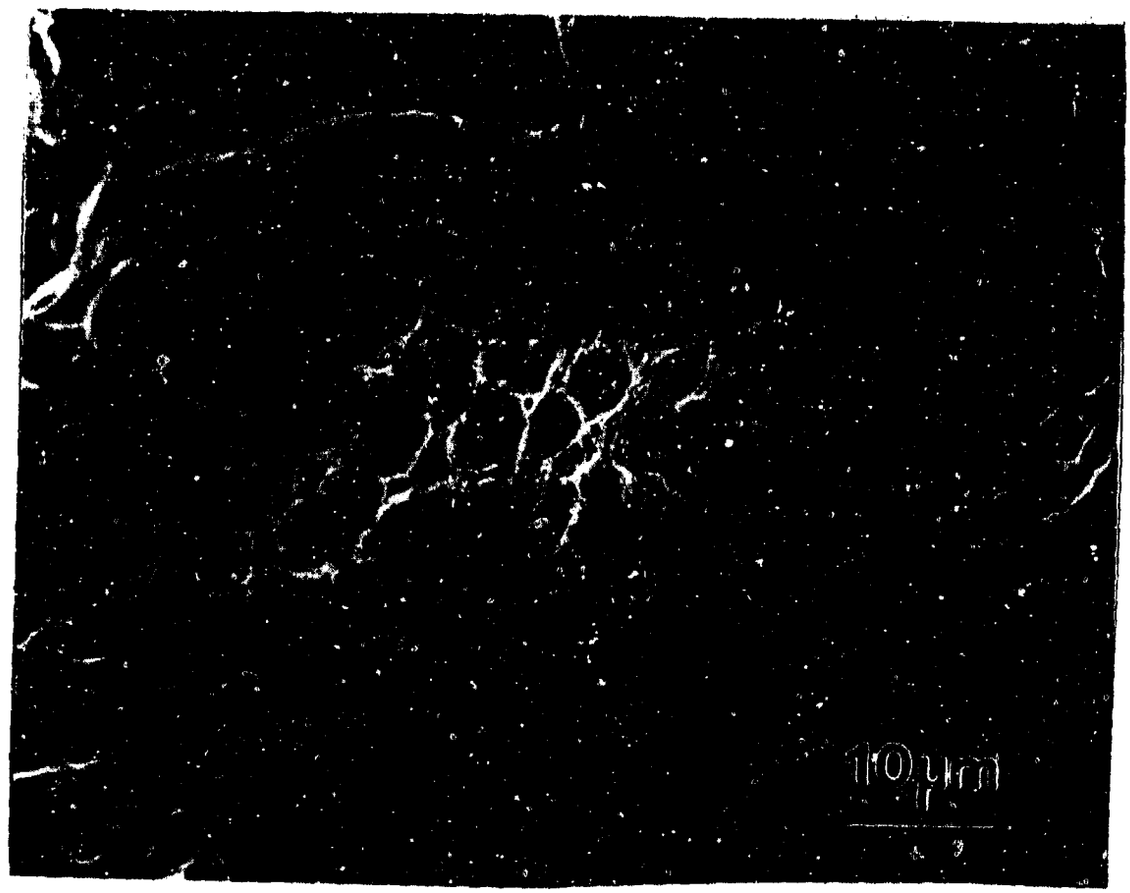


Fig. II,4-1(a). This micrograph of a Ti-6Al-4V tensile sample contains examples of the three major fracture surface features associated with localized melting during separation; an open surface shear zone, transition dimples and mixed mode spheroidized dimples with associated spheroidized surface debris.

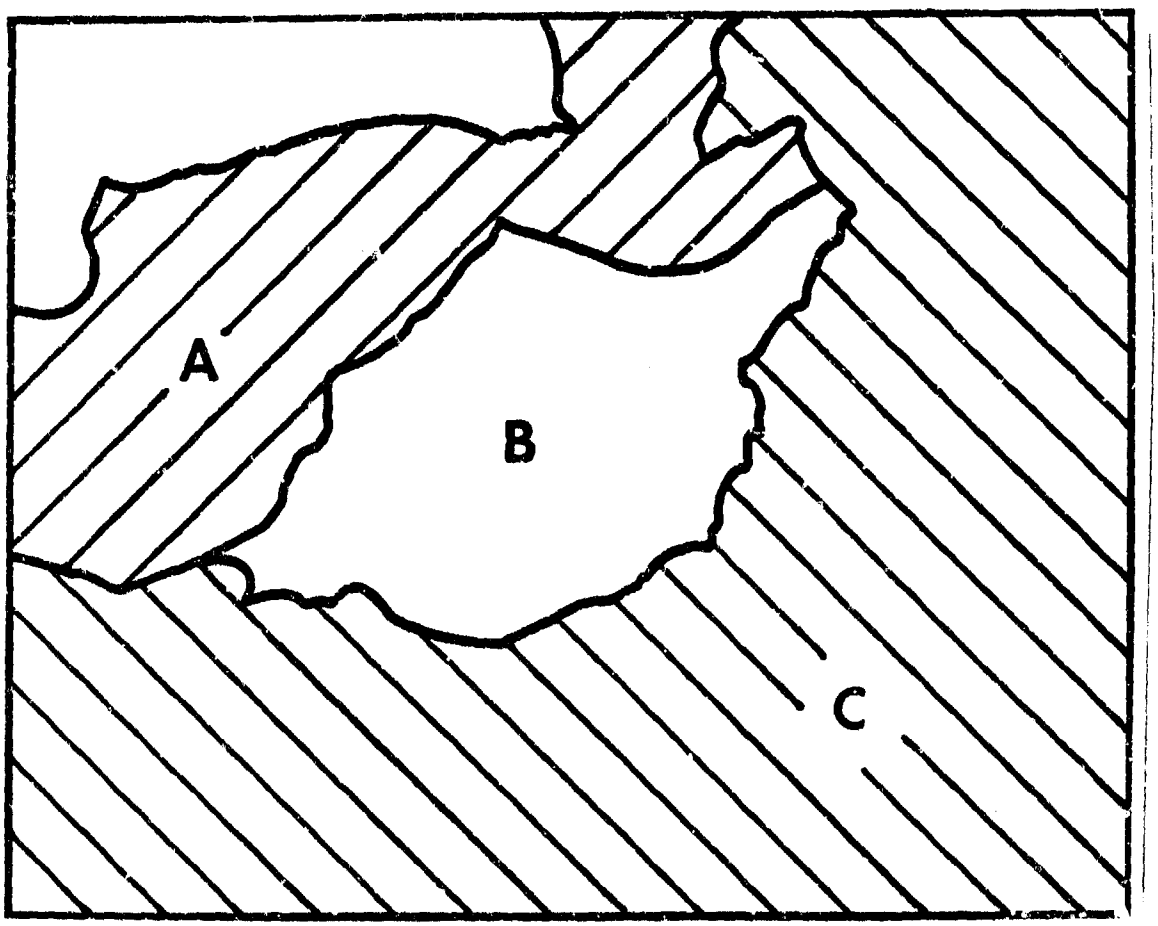


Fig. II,4-1(b). This is a schematic diagram which defines the locations in (a) of (A) the open-surface shear zone, (B) mixed mode spheroidized dimples with associated spheroidized surface debris and (C) transition dimples.

Fig. II,4-2. This micrograph shows a section below a region of localized melting on the shear lip of a Ti-8Mn tensile sample fracture surface. The deflection of acicular α platelets clearly shows the localized shear directly below the unusual surface features.

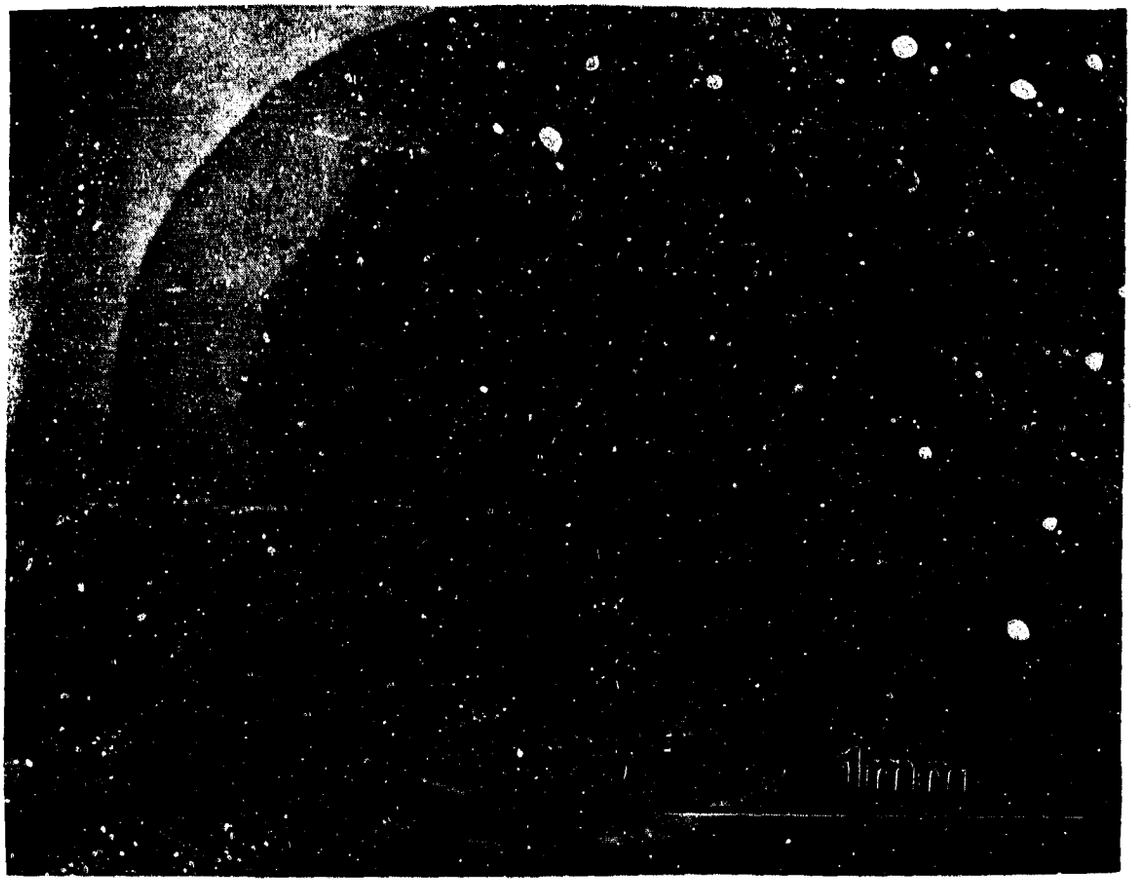

Fig. II,4-3(a). Low magnification micrograph of the fracture surface of a quasi-static AISI 4340 steel tensile sample with a 435°C temper showing a well-defined shear lip and a region of radial cracking surrounding the central area of fibrous fracture.

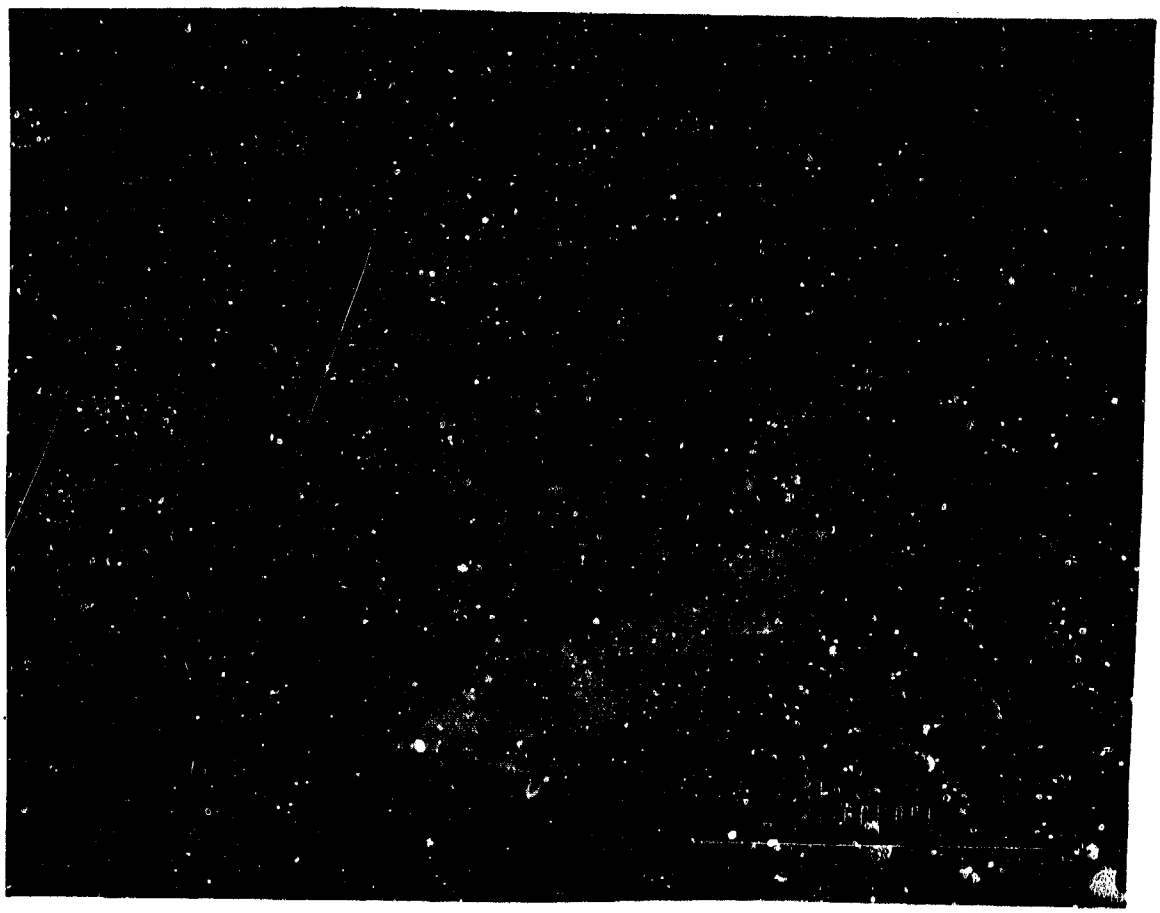

Fig. II,4-3(b). Low magnification micrograph of the fracture surface of a high strain rate (applied rate $8.3X10^{3}d^{-1}$ AISI 4340 steel tensile sample with a 435°C temper. Note the total absence of radial cracking.

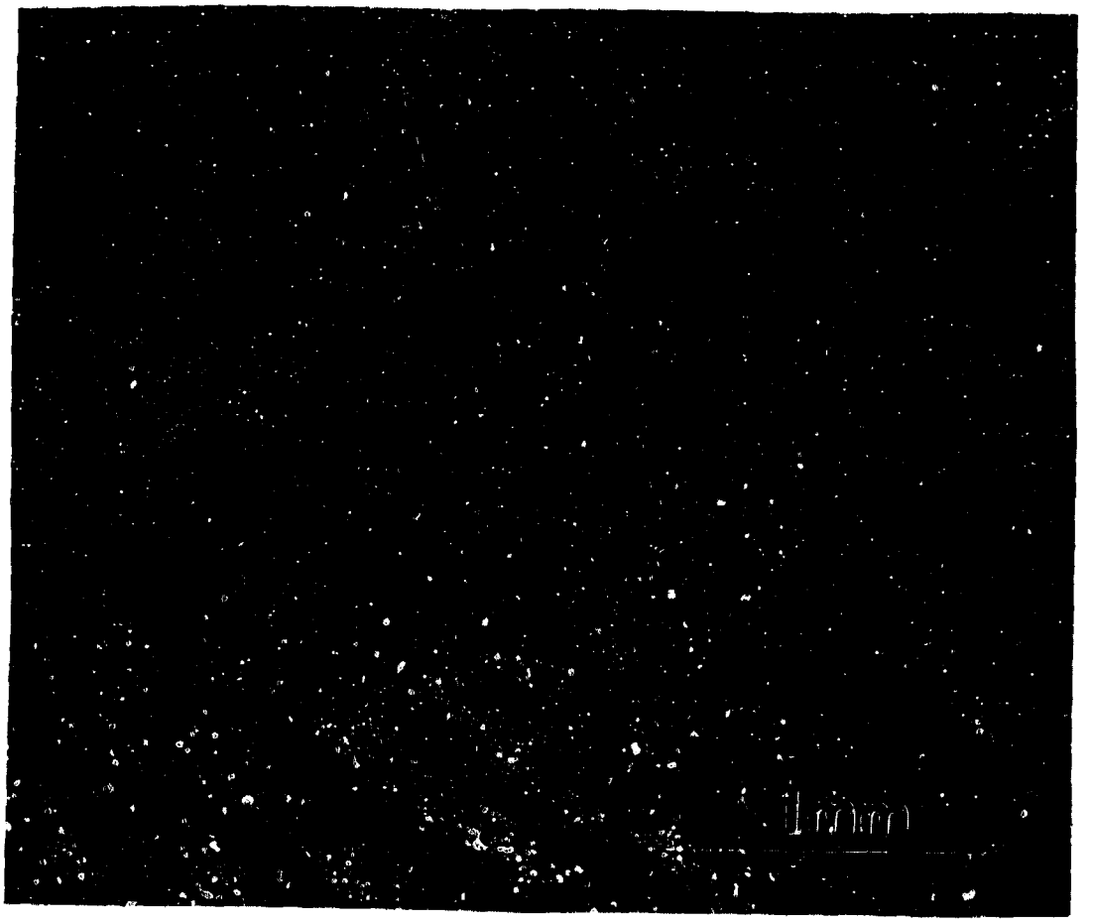

Fig. II,4-3(c). Low magnification micrograph of the fracture surface of an AISI 4340 steel tensile sample fractured using an ultrasoft set-up in which a large spring is placed in series with the sample, decreasing the machine stiffness by a factor of approximately 500. Note the absence of radial cracking as in the high rate sample surface shown in (b).

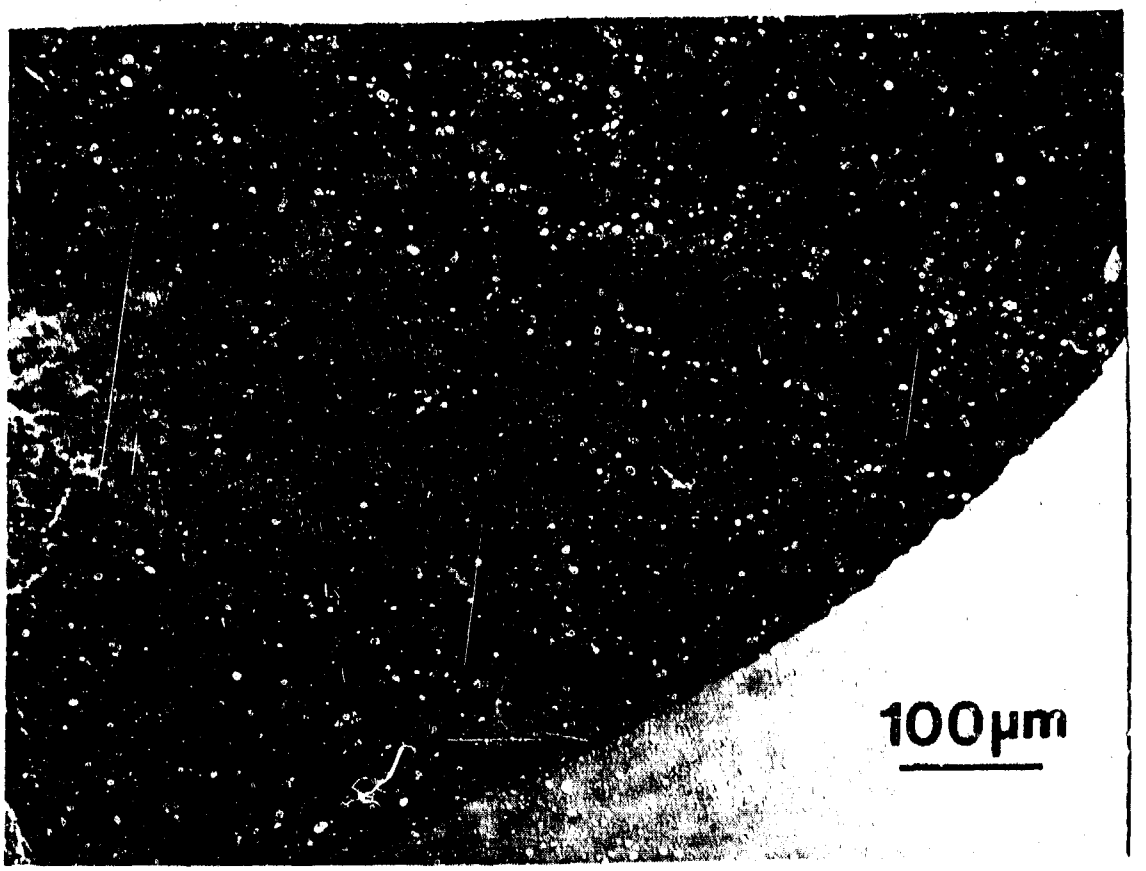


Fig. II,4-4(a). Micrograph of a portion of the shear lip of a quasi-static AISI 4340 (435°C temper) tensile sample which contains regions of localized melting (arrow indicates region contained in (b)).

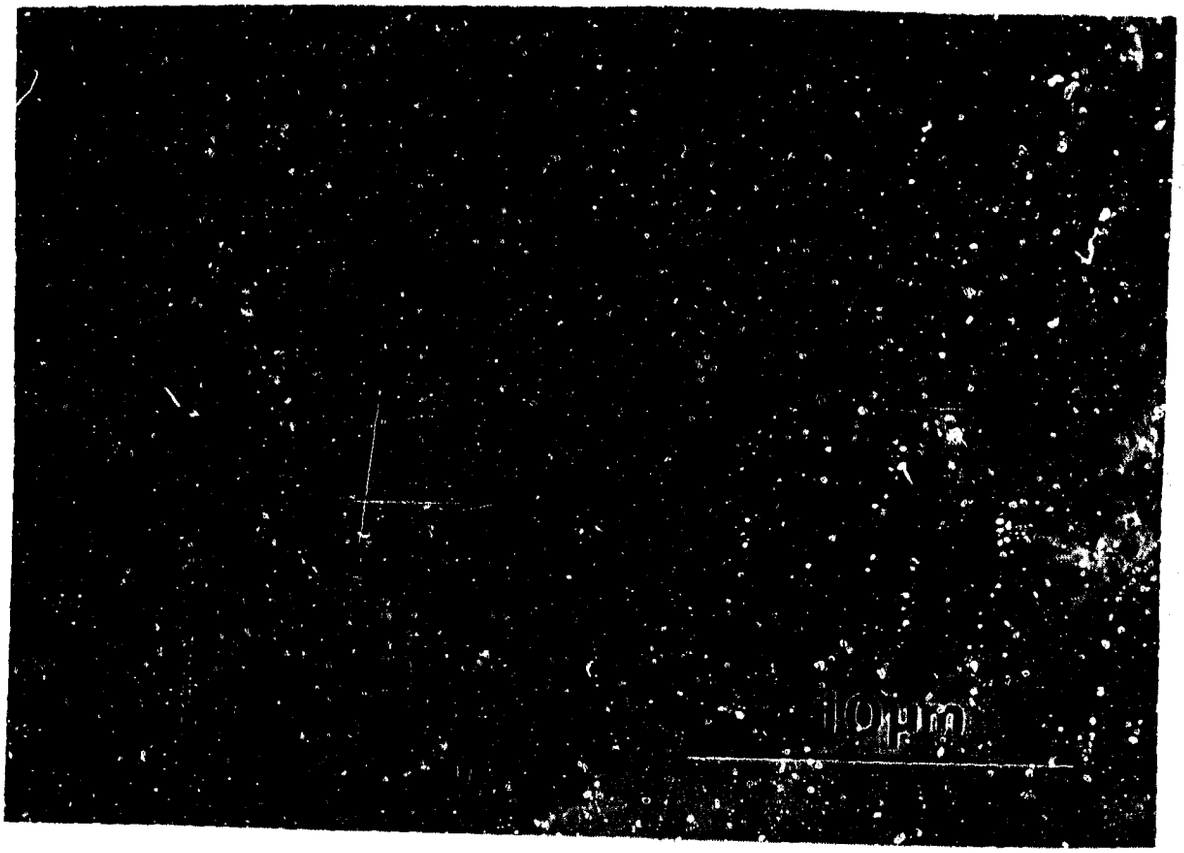

Fig. II,4-4(b). Higher magnification micrograph of a portion of the shear lip shown in (a) which contains regions of localized melting (indicated by arrows).

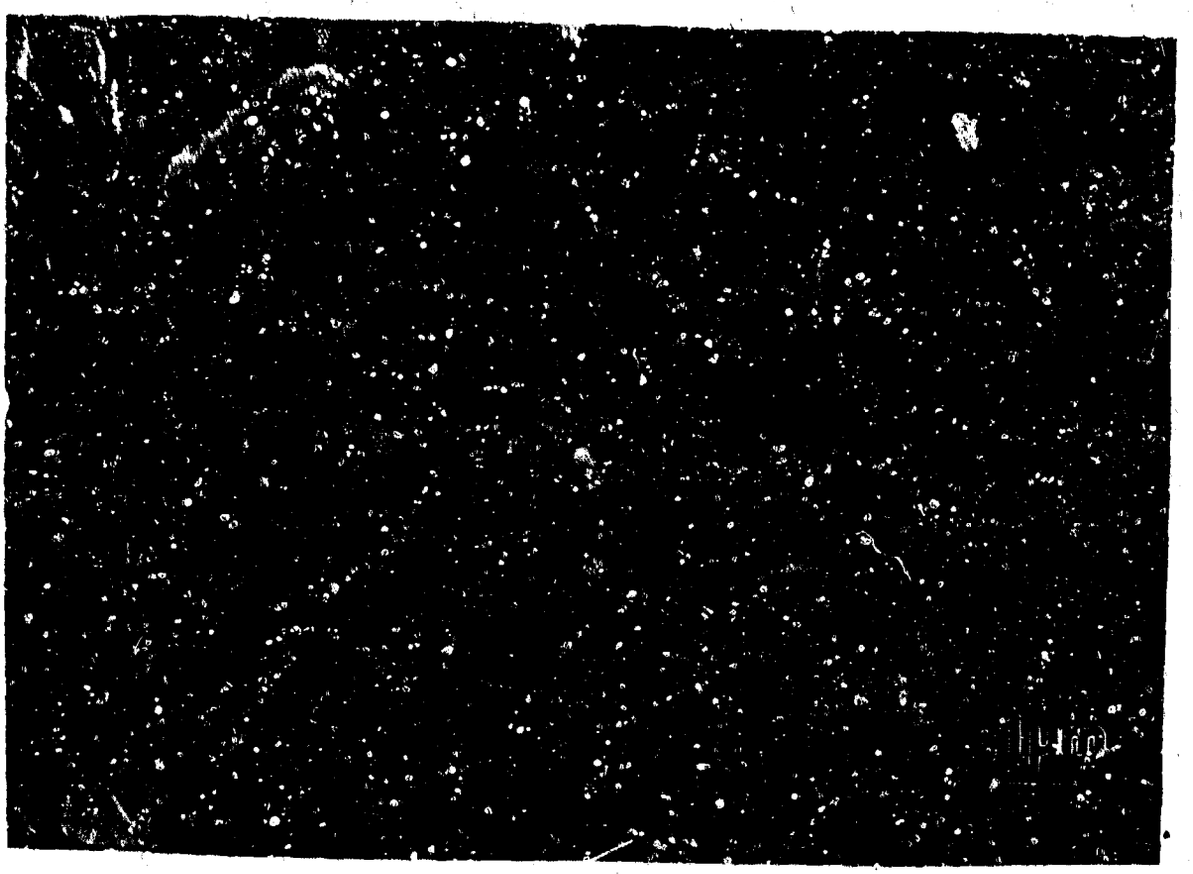

Fig. II,4-4(c). High magnification micrograph of one of the regions of localized melting shown in (b) which is directly below a smoother-than-normal band which is an example of an open-surface shear zone on a 4340 steel fracture surface.

In both cases the locally melted regions are made up of spheroidized dimple walls surrounded by shear dimples. The melted material appears different from the surrounding material not only because of the spheroidized features but also because the dimples appear to have formed in a different mode form the highly sheared surrounding dimples. This makes the melted areas stand out from the more typical surrounding shear dimples. Also, in both these samples and the earlier titanium samples the melted features are adjacent to smoothly sheared areas. In the titanium samples these sheared areas are almost completely dimple-free, as can be seen in the open surface shear zone in Figure II,4-1, while in the steel samples the sheared areas are smooth but contain holes. These areas are identical to "holey smeared" regions which have previously been associated with the initiation of adiabatic shear in high rate shear experiments on 4340 steel (33-35).

(iv) Discussion.

The first question which arises from the results is, "Why do the quasi-static test samples contain radial cracks while the radial cracks are absent in the high rate and ultra-soft test samples?" Radial cracking in steels has been extensively investigated, not only in tensile samples but also in various types of service failures (36-38) and it has clearly been shown to result from rapid crack growth and it is frequently the dominant fracture surface feature in failures which result from high rate failures such as those caused by impact and explosive loading. This might imply that radial cracking should be expected in the high rate and ultra-soft test samples, where the elongation rate immediately prior to separation is much greater than in the case of the quasi-static tests, but this is not the case.

The reason why the radial cracks are found only in the normal quasi-static test samples is that a higher applied strain rate does not necessarily cause a higher crack propagation rate. In a test system such as the one used in this study the elastic energy stored in the loading train (load frame, load cell, grips and sample) result in elastic deformation in the direction of the tensile axis which is large compared to the amount of displacement which occurs during separation. In our normal quasi-static test system (without the large spring in series with the sample) the stiffness of the total loading train is about $2.5 \times 10^7$ N/m. Since separation occurs very rapidly, even for quasi-static tests, the decrease in load

with elongation due to elastic relaxation is obviously less than the decrease in load bearing capacity with elongation during separation. Under these conditions where the driving force for crack propagation comes primarily from elastic energy stored in the test system the crack propagation rate is controlled primarily by the amount of localized ductility at the tip of an advancing crack, i.e. in the "process" and plastic zones of the crack tip, not by the applied strain rate (crosshead speed).

Crack tip ductility is the basic mechanism responsible for the ductile/brittle transition with temperature, and the increase in ductility with ambient temperature is also the key to suppression of radial cracking in the high rate and ultra-soft tests. Studies of 4340 Charpy v-notch samples show that the fracture toughness, as measured by absorbed impact energy, increases dramatically as the ambient temperature increases through the ductile/brittle transformation temperature range (39). Similarly, fracture surfaces of 4340 tensile samples show that below the ductile/brittle transformation temperature range radial cracking makes up the majority of the interior crack area (37,38) and as the temperature increases through the ductile/brittle transformation temperature range, the percentage of area displaying radial cracking continuously decreases until the radial cracks completely disappear above the transition range.

When metals undergo plastic deformation a very large percentage of the energy of deformation is non-conservative and, by means of drag forces generated by the interactions of dislocations with phonons, electrons and other dislocations, this energy takes the form of heat.

As the strain rate of a deforming system increases heat losses through conduction become less significant in the calculation of temperature rise and at high enough rates the losses become negligible and the system behavior is essentially adiabatic. If the strain rate is high enough that phonon drag forces and elastic wave interaction are significant, however, the quasi-static approximation of material behavior becomes inaccurate and dynamic effects must be considered. In between the strain rates where heat conduction and dynamic effects are significant there is a window of rates for which nearly quasi-static and adiabatic conditions exist. This window of strain rates depends on the size and materials properties of the deforming volume and can be approximated by

$$\frac{K}{L^2} < \dot{\gamma} < \frac{\sigma}{L\sqrt{\rho G}} \qquad [18]$$

where $\dot{\gamma}$ is the strain rate, $\sigma$ is the flow stress, K is the thermal diffusivity, L is the characteristic length of the deforming region, $\rho$ is the density and G is the shear modulus (40). Using the values given in Table III for our 4340 steel samples this

---

TABLE III

PHYSICAL CONSTANTS OF AISI 4340 USED FOR CALCULATIONS

Density (rm. tmp.): $7.83 \times 10^6$ Kg/m$^3$ [21]

Thermal Conductivity (rm. tmp.): 37.5 J·m/sec·m$^2$·°C [21]

Thermal Diffusivity: $1.07 \times 10^{-5}$ m$^2$/sec

Shear Modulus (rm. tmp.): $7.58 \times 10^4$ MPa [22]

Specific Heat (rm. tmp.): $4.48 \times 10^2$ J/Kg·°C [21]

---

places the approximate strain rate limits for quasi-static adiabaticity in the overall gage length between 0.074 sec$^{-1}$ and $4.1 \times 10^3$ sec$^{-1}$ and for the neck region between around 0.32 sec$^{-1}$ and $8.5 \times 10^4$ sec$^{-1}$. The high-strain rate tests (where the applied rates are between $1 \times 10^2$ sec$^{-1}$ and $3 \times 10^3$ sec$^{-1}$) fall within these limits, as do the post-UTS strain rates of the ultra-soft tensile tests, where neck formation and fracture occurs well under one second.

Assuming quasi-static adiabatic conditions and also assuming that 86.5% of the energy input into the sample during uniform elongation causes heating, we can approximate adiabatic temperature rise to a particular plastic strain $\varepsilon_f$ using the following equation

$$\Delta T = \frac{0.865}{\rho c} \int_0^{\varepsilon_f} \sigma_y \, d\varepsilon_p \qquad [19]$$

where $\Delta T$ is the temperature rise, $\sigma_y$ is the yield stress, $\varepsilon_p$ is the plastic strain, $\rho$

is the density and c is the specific heat. If we assume that the true stress-true strain behavior of the samples can be approximated by the Holloman strain hardening relationship (41)

$$\sigma = K\varepsilon^n \qquad [20]$$

then the adiabatic temperature rise equation reduces to

$$\Delta T = \frac{K}{c\rho(1+n)}\varepsilon_t^{(1+n)} \qquad [21]$$

where n is the experimentally determined workhardening coefficient.

Unfortunately these mathematically simple analyses require a true stress/true strain curve which can be accurately fit using the Holloman relationship. In the case of our tests the extensive post-UTS elongation make true stress/true strain information difficult to ascertain. The standard method of approximating post-UTS stress/strain information involves the assumption of the von Mises yield criterion (42) resulting in the Bridgeman correction (43). This analysis, however, also assumes a neck shape which can be approximated by a section from the center of a toroid, i.e. a portion of a doughnut hole, and the profiles of our post-fractured samples show that this is not nearly the case.

To more accurately measure the energy of deformation the load/elongation curves which resulted directly from the testing were divided into three different regions; the elastic regions prior to plastic deformation, the uniform elongation regions prior to neck initiation, and the post UTS region which represented the formation of the neck to fracture. Integration of the area below the two plastic deformation regions gives a good approximation of the strain energy put into the samples during straining. It should be noted that this analysis assumes that the load elongation curves for the quasi-static tests are approximately the same as those for the high strain rate and the ultra-soft tests, which are not available. The similar shape of all of the samples after fracture is a relatively good indication that this is a reasonable assumption, and any differences which might occur are probably not significant to the accuracy of this model.

To approximate the temperature rise resulting from plastic deformation we

also need to know the volumes of the deforming regions. Calculating the volume of the gage lengths is obviously trivial, but the volume of the neck is not so straightforward. Using the profile projector, the profiles both sides of the sample necks were graphically re-assembled to approximate the neck shapes at the point of separation. These shapes can then be numerically integrated to give values of the total neck volumes.

Now we have approximate plastic deformation energy values and approximate deforming volume values so we can use a simplified version of eq. [19] to estimate the temperature rise.

$$\Delta T = 0.865 \frac{E_{PL}}{C\rho V} \qquad [22]$$

There are two different cases for the temperature rise calculations; the high strain rate samples and the ultra-soft samples. The difference occurs because while the high strain rate samples deform completely under nearly adiabatic conditions, the ultra-soft samples are only nearly adiabatic after UTS, i.e. during neck formation. In the calculations this means that the temperature rise of the high strain rate samples is the sum of the uniform and the post-UTS increases while the temperature increase for the ultra-soft samples is only that generated during post-UTS deformation.

Using load/elongation information for a typical quasi-static sample the uniform deformation plastic work energy can be estimated to be about 5.75 Joules while the post-UTS plastic work energy is about 12.2 Joules. Volume calculations estimate the gage volume to be about 119 $mm^3$ and the neck volume to be about 42 $mm^3$. Using these values with equation [22] gives us an approximate temperature rise of 13°C during uniform elongation and of approximately 81°C during necking. This makes the total temperature rise at the center of the neck about 86°C for the high strain rate samples and about 74°C for the ultra-soft samples. These calculations are in general agreement with in-situ temperature measurements of steel tensile samples made using a high-speed infrared thermometer (44).

While a temperature rise of between 74°C and 86°C might cause a small amount of thermal softening in most structural metals, this temperature

increase is particularly important for the 4340 tensile samples used in this study because the ductile-brittle transformation temperature range is near room temperature. Experiments conducted at various ambient test temperatures have shown that the transformation temperature range for AISI 4340 steel with a 435°C temper lies between -160°C and approximately 60°C (14). Herein lies the explanation for why the radial cracking is absent in the high-rate and ultra-soft tests, since the increased temperature in the neck prior to separation causes the material to fracture in a purely ductile manner, while in the quasi-static tests the separating material temperature falls within the ductile/brittle transformation range and the material fractures in a partially brittle manner.

Although adiabatic heating during general gage deformation and necking can cause an important temperature increase, it is not the mechanism by which localized melting occurs at separation, as shown in these experiments in which the samples adiabatically heated during overall straining were not the samples which contain locally melted surface areas.

The appearance of localized melting in the shear lip areas of 4340 samples is in many ways similar to that of titanium alloys. Spheroidized dimple walls and surface debris are found in patches surrounded by shear dimples, as seen in Figure II,4-4c. These patches of local melting are also typically adjacent to relatively smooth surfaces which are, by all appearances, identical to "holey smeared" regions which have been associated with the initiation of adiabatic shear in high strain rate shear tests of 4340 steel (33-35). Signs of possible adiabatic shear are not unexpected since highly localized and possibly adiabatic shear has been found to accompany the localized melting in both Ti-8Mn and Ti-6Al-4V tensile samples.

Another significant difference in the local melting in the 4340 samples is the relative scarcity of the melted areas as compared to the titanium alloys. Melting in these samples occurs not only over smaller local areas (by a factor of approximately 3-5) but also occurs less frequently than in the titanium alloys.

The parallel between localized melting and radial cracking is of great interest, since it emphasizes the need for high crack propagation rates. This is in agreement with a recent study in which localized melting in Ti-6Al-4V tensile samples was suppressed by heat treating to a colony $\alpha$ microstructure, apparently because of an increase in crack path tortuosity and a resultant decrease in crack

propagation rate (6). A recent computer model of heating at a moving crack tip (5) has shown that dislocation production rates are critical in achieving high crack tip temperatures and it may be a lowering of these production rates that inhibits localized melting. An important point to note is that the radial cracking indicates rapid crack propagation in the central crack portion of the sample while the melting is found in the shear lip. This is an indication that, as might be expected, the separation rate of the central crack influences the shear lip formation rate.

High crack propagation rates have two major effects on local temperature rise, both of which result from an increase in the local strain rate. First, the shorter time of deformation decreases the amount of heat conducted away from the separating surface, making the conditions more nearly adiabatic. Second, increases in strain rate, especially at the high rates which occur during separation, cause an increase in the instantaneous yield stress, thereby increasing the amount of energy resulting from the same amount of strain.

It should be noted that general heating of the gage volume, localized heating of the neck, and heating during localized and possibly adiabatic shear all predicate the heating at final separation which occurs during the rupture of the ligaments which surround the growing voids. Rupture of these ligaments occurs at extremely high strain rates and the total plastic strain involved is very large, making the total energy density of the ligaments during rupture very high. Temperature increases in the separating ligaments must be, once again, added to the prior temperature increases. Taking this into consideration it appears that high strain rates and high ambient local temperatures in the immediate vicinity of the separating ligaments are the critical conditions for localized melting at final separation.

(v) Conclusions

1. Under certain conditions, specifically those which cause high crack propagation rates, localized melting occurs on the shear lips during the separation of 4340 steel tensile samples.
2. Localized melting can be suppressed by increasing the ambient temperature of the separating volume above the ductile/brittle temperature transformation range. In this study the temperature increase was caused by heating of the gage and neck volumes during elongation.
3. In the 4340 samples used in this study the presence of locally melted

regions has been shown to accompany radial cracking, indicating that the mechanisms responsible for the local melting are also associated with rapid crack propagation through the central portion of the sample.

(This page intentionally left blank.)

(This page intentionally left blank.)

# APPENDIX

## A1. Characterization of Fracture Surfaces.

The investigation of fracture surfaces with scanning electron microscopes (SEM) has become a standard procedure. However, only when stereo-pairs are being evaluated, can a meaningful interpretation of the often complex topography of a fracture surface be attempted. The development of a semi-automatic stereo device by this group has been reported earlier (45,46). This instrument has been used extensively for determining the 3-D topography of fracture surfaces throughout the studies under this contract.

However, a new task arose, namely the quantitative assessment of "melted" dimple areas and other unusual surface features in the fracture surface topography (see for definitions Table A1,I).

TABLE A1,I. Definitions of Unusual Features on Fracture Surfaces of Selected Tensile Loaded Alloys (47).

| | Microstructural Classification | Definition |
|---|---|---|
| 1. | Dimple groups heated above melting point, or "melted dimples" | Areas of shallow dimples. Dimple walls are outlined with small solidified metal droplets at the top, while the dimple bottoms are covered with tiny specks of solidified metal (like a spray). |
| 2. | "Transition Dimples" | Dimples with low walls lying on a common shear plane |
| 3. | "Open Surface Shear Zones" | Dimple-free, flat surfaces of considerable length and limited width found at the perimeters of some shear areas. |

The research reported in Sections II,1 and II,2 provided new theoretical and experimental information against which a quantitative comparison could now be made. The results of that study follows in Section AII. Here, a brief description of

the techniques of observation and counting will be given.

As a first step, a composite picture of the fracture surface was produced with the SEM at a 40X magnification. The composite micrograph was used (i) as a "road map," and (ii) as a base for a real measurement. This was accomplished by putting a plastic overlay on the composite picture and marking in transparent color the surface categories listed in Table A1,I. These were obtained from micrographs taken at magnifications between 1,000X and 3,000X. All observations were checked on the matching fracture surface and, in general, the areas determined agreed within a 20% error margin. The special features measured in this fashion were determined as a function of the macroscopic strain rate as reported in the next section. An example of a composite micrograph with the features marked on the surface is given in Figure A,1-1.

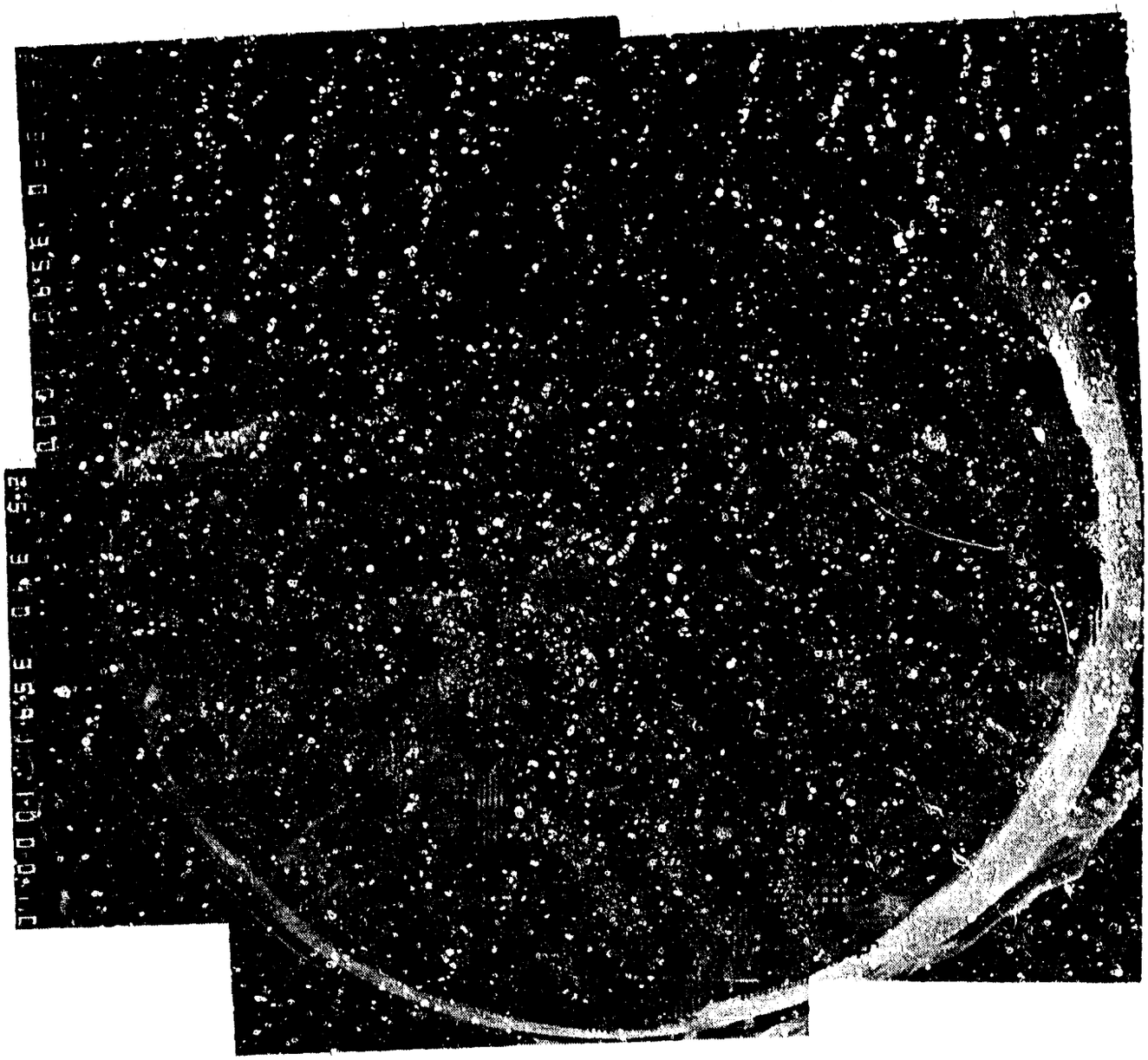


Fig. A1-1. Low magnification composite photo of Ti-10V-2Fe-3Al tensile sample fracture surface with portions and approximate sizes of areas of interest indicated.

## A2. The Effect of Applied Strain Rate on the Extent of Localized Shear Separation

Once the fracture surface features resulting from unstable shear separation (open surface shear zones, transition dimples and localized melting) had been investigated to the point that they could be unambiguously defined, this opened up the possibility of studying the effect of strain rate on the extent of localized shear separation. Although this phenomenon occurs even at quasi-static applied rates, indicating that the final unstable separation is driven by the elastic energy stored in the test system as a whole, the effects of strain rate on the pre-separation deformation of the sample might have a measurable influence on the fracture surface features of interest.

### Material Selection

The material selected for this investigation was Ti-10V-2Fe-3Al primarily because previous investigations had shown that (i) the tensile samples do not form a concentrated neck prior to separation, (ii) localized melting can be found on the fracture surfaces and (iii) small increases in temperature (50°C or so) do not have any dramatic effect on the mechanical or fracture properties. Concentrated necking was avoided because the moderate temperature increases which accompany adiabatic necking can be significant, thereby possibly causing unwanted differences in the "ambient" temperature in the region of incipient separation between quasi-static and high-rate samples. Similarly, materials which have different deformation or fracture characteristics at slightly elevated temperatures (such as the ductile/brittle transformation temperature in some steels) could also add an undesirable complication to the interpretation of the effects of high applied strain rate.

### Heat Treatment

Heat treatment of the samples, which was conducted in an argon atmosphere, started with a 3 hour solution treatment at 780°C followed by a water quench. Samples were then aged at 500°C for 1 hour and cooled in flowing argon. This resulted in a microstructure of large lamellar $\alpha$ precipitates, which caused the subsurface deformation to be clearly indicated by the deflection of the precipitates.

### Sample Configuration

The samples used were of the double gauge type, as shown in Figure A2-1,

in which, during a test, the smaller diameter gauge area deforms elastically and then plastically while the larger diameter gauge area deforms only elastically. Prior to testing, strain gauges attached to the larger elastic gauge area are calibrated to loads below the elastic limit of the smaller plastic gauge area. This provides for accurate load measurement directly adjacent to the plastically deforming portion of the sample, thereby effectively reducing the elastic wave effects which can obfuscate the true values at high loading rates. Strain gauges are also attached to the smaller diameter plastic gauge to provide information on strain and strain rate.

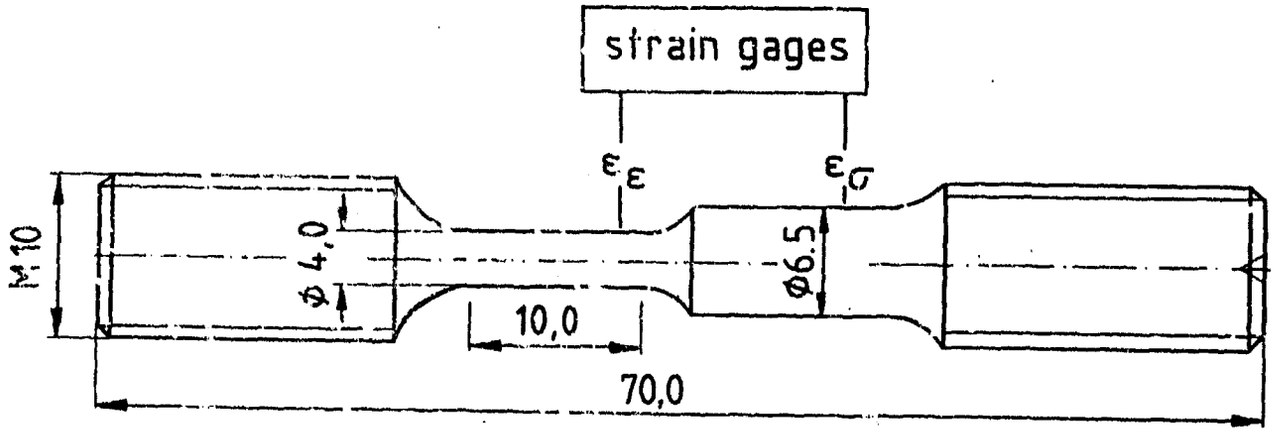


Fig. A2-1.Geometry of samples used in high-rate tensile tests.

Tensile Testing

Low strain rate tests were performed with a universal servo-hydraulic testing machine and the high strain rate tests were performed at the Fraunhofer Institut (Bremen-Lesum, Germany) using a rotating wheel machine. For the high-rate tests signals from the strain gauges on the elastic and plastic regions of the samples were recorded using high speed digital storage oscilloscopes and the resulting data files were then used subsequently to construct stress/strain curves.

Tensile Results

Although there is some scatter in the data, it is obvious from Figure A2-2 that the true ultimate tensile strength ($UTS_{true}$), the 0.2% offset yield strength, the reduction of area, and the elongation to fracture all generally increase with

increasing applied strain rate. The fact that the reduction of area is consistently greater than the elongation to fracture is an indication that some strain localization in the gauge length does occur, but this difference is not large enough to indicate a concentrated neck, as also verified by the appearance of the fractured samples.

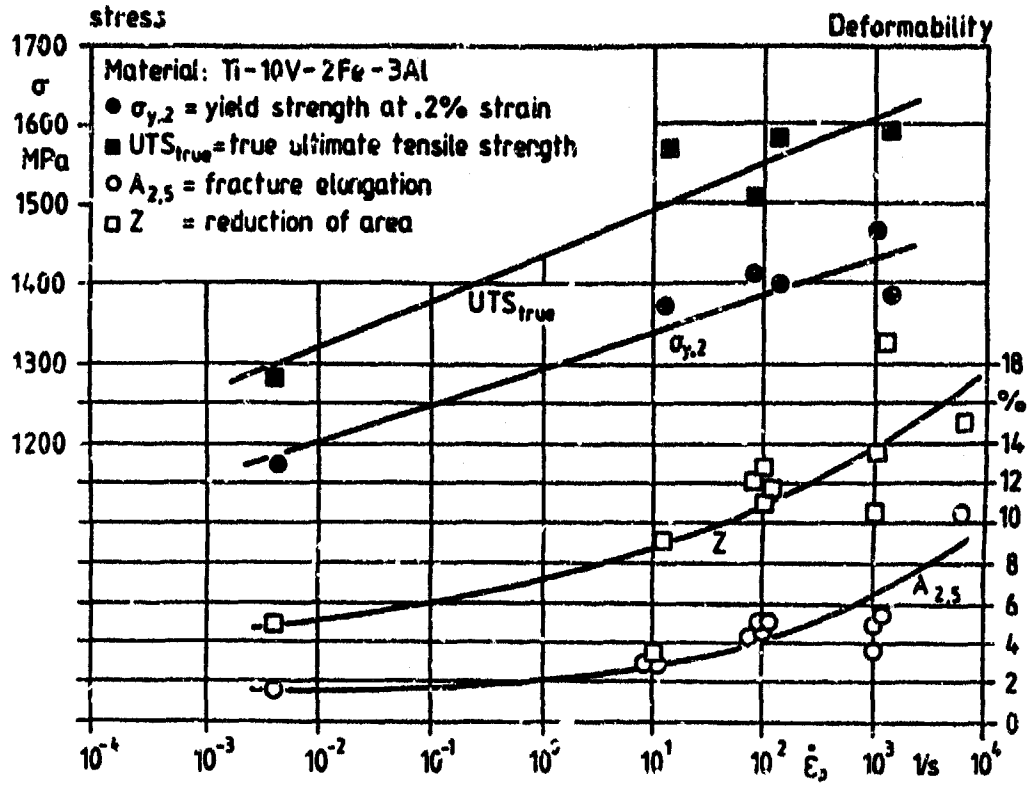


Fig. A2-2. The effect of applied strain rate on the tensile properties of Ti-10V-2Fe-3Al.

General Fracture Surface Appearance

The fracture surfaces which result from the quasi-static and dynamic tensile tests have a minor but discernable difference in local roughness, as noted in an earlier investigation(2) of tensile samples made of the same alloy. All of the fracture surfaces have a distinct shear nature, being predominantly tilted at an approximately 45° angle to the tensile axis, although not necessarily in a single plane. Some of the surface areas are intergranular, but the overall intergranular area is typically less than about 10-15%. The surfaces are covered with ductile

dimples (except for the open surface shear zones with no signs of cleavage.

Fracture Surface Quantification

Results of the fracture surface analyses are summarized in Fig. A2-3. This graph plots the area coverage of the different features in terms of measured area and percentage of area as a function of the applied strain rate. Although the trends are not uniformly monotonic, the indications of increases in areas with increasing applied strain rate are obvious.

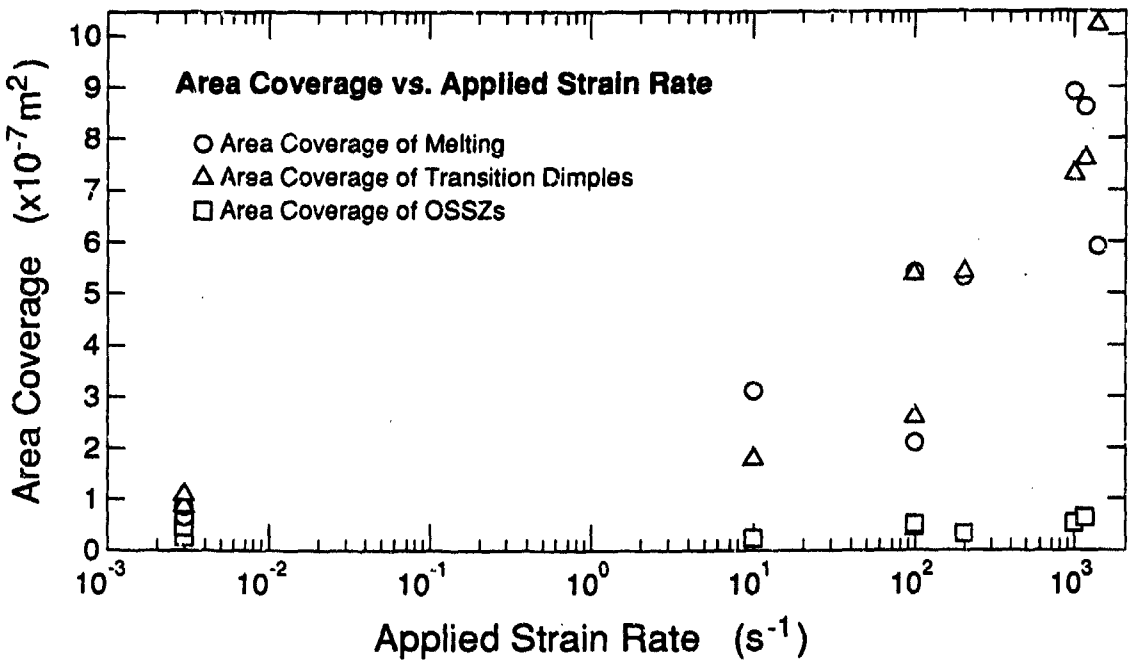


Fig. A2-3. The effect of applied strain rate on the area coverage of various features of interest on the fracture surfaces of Ti-10V-2Fe-3Al tensile samples.

Discussion

In the previously presented model of separation transition dimples and locally melted regions are formed by separation through planar bands of concentrated shear which are a result of material instabilities during the final shear separation. Since the sections cut through the fracture surfaces parallel to the tensile axis show very little indication of concentrated shear other than that directly below the fracture surfaces it is likely that the sum of both the transition

dimple areas and the locally melted areas on any particular fracture surface is an indication of the extent of the unstable shear which occurred during the separation of that particular sample. Figure A2-4 is graph of the sum of the transition dimple and locally melted areas for the tensile samples investigated. This graph shows a definite trend of increasing area coverage with increasing applied strain rate, indicating that the extent of unstable shear increases with increasing applied strain rate.

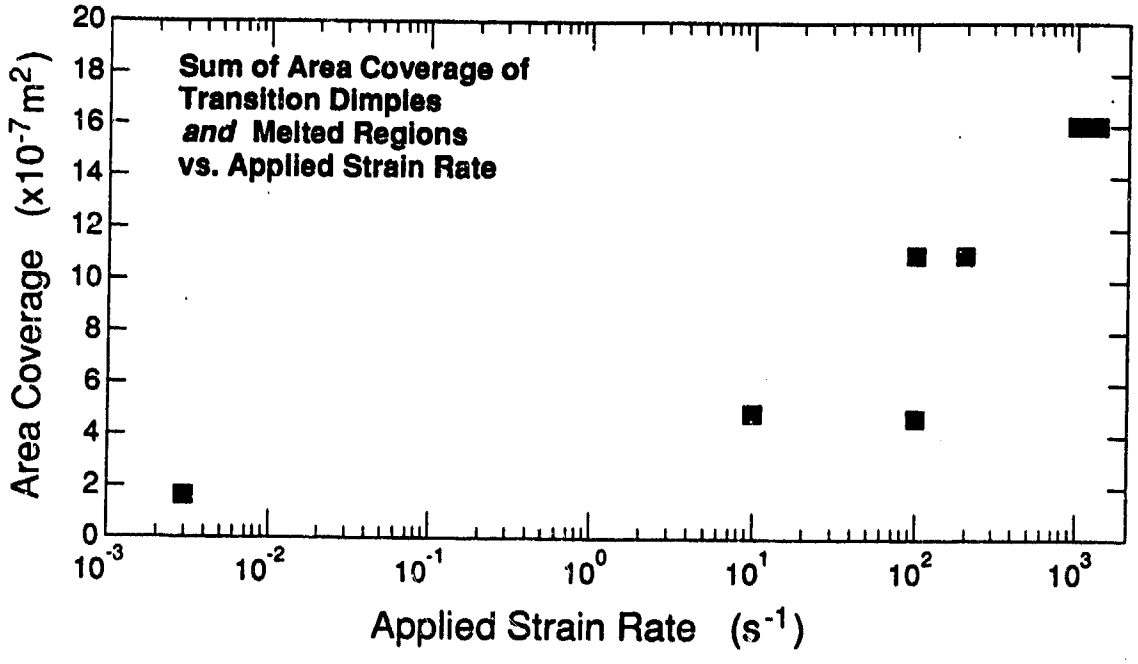


Fig. A2-4. Area coverage of the sum of the localized shear induced fracture surface features as a function of applied strain rate.

One should be careful not to immediately equate the applied strain rate with the effective crack propagation rate. Rather, the effect of the applied strain rate may be to cause a different material condition at the onset of separation, thereby only indirectly influencing the separation process. The interaction between applied strain rate and the final fracture mechanisms is, therefore, rather subtle and these current results hold considerable information which is still undergoing scrutiny and will result in a publication to be co-authored by D. D. Makel, H.G.F. Wilsdorf, and B.-O. Reinders and H.-D. Kunze of the Fraunhofer Institut.

A3. Fracture Surface Investigations of High Strength Alloys

As a compliment to the work done on titanium alloys Ti-10V-2Fe-3Al, Ti-6Al-4V and Ti-8Mn a number of other high strength alloys were strained to fracture and the resulting fracture surfaces scrutinized for signs of localized melting or transition dimples. All tests were run at approximately $5x10^{-4}s^{-1}$ applied strain rate at room temperature, except where noted.

Superalloys

INCO Alloy 600

The first superalloy tested was INCO Alloy 600, a very popular and well-established industry standard. These samples workhardened significantly, resulting in very high UTS levels, and the fracture surfaces were beautiful examples of cup-and-cone separation. Although there were very large, regular shear areas covered with ductile dimples, no transition dimples or localized melting were found on any of the surfaces.

René 41

Like the INCO Alloy 600 samples, these samples workhardened to very high UTS values. Separation occurred very dramatically in these samples, in one case actually shattering a large grip insert. The resulting fracture surfaces were perpendicular to the tensile axis and almost completely intergranular (typically referred to as "rock candy" type surfaces). Although the grain boundaries did show some fine ductile features and intergranular ductile separation could be found in some highly localized regions near the outer edges, no indications of transition dimples or localized melting were observed.

Steels

AISI 4340

Samples made of AISI 4340 (350°C temper) were tested and the cup-and-cone fracture surfaces were found to contain all of the fracture surface features indicative of concentrated shear and localized melting, and also central crack areas with radial cracking, an indication of high crack propagation rates. Subsequent testing in an ultra-soft test setup and at high applied strain rates resulted in fracture surfaces completely devoid of transition dimples, localized melting or radial cracking. This reduction in crack propagation rate at elevated strain rates was determined to be due to an adiabatic increase in the neck temperature prior to separation which raised the temperature in the region of

incipient separation above the ductile/brittle transformation temperature range. Results of these investigations have been written up in a paper which has been accepted for publication in "Materials Science and Engineering."

HY80

This alloy had moderate tensile properties and the fracture surfaces were primarily cup-and-cone, although considerably less regular than the Alloy 600 or 4340 samples. These surfaces did not contain radial cracks or any of the concentrate shear features of interest. Since radial cracking and localized melting were only found in the 4340 samples fractured at temperatures within the ductile/brittle transformation temperature range (not above) the HY80 samples were tested at decreasing temperatures in an attempt to increase the crack propagation rate. At temperatures slightly below -50°C the samples did develop radial cracks during separation, but subsequent investigations of the fracture surfaces in the SEM did not reveal any transition dimples or localized melting.

W1 Tool Steel

Samples of W1 tool steel were very difficult to test, as they tended to break in the grips after almost no plastic deformation. Fracture surfaces appeared generally smooth and featureless at low magnifications and holey and brittle at higher magnifications. No indications of any features of interest could be found on the surfaces.

Aluminum

7075

Samples made of 7075 aluminum showed good strength and moderate toughness. The fracture surfaces were very irregular, with the most outstanding features being the obvious void initiation sites being located at cracked hard particles. These surfaces showed some open surface shear zones but no transition dimples or localized melting.

Al-2%Cu

Fractured tensile samples of Al-2%Cu, peak hardened to contain G.P. zones were observed in the SEM for signs of localized melting. These surfaces were nearly all shear, with very little central crack area and they showed no signs of transition dimples or localized melting.

A summary of the results SEM analyses of these alloys and the titanium alloys is shown in Table A3-I.

TABLE A3-I. Summary of Fracture Surface Investigations

| Material | Test Condition | Localized Melting |
|---|---|---|
| **Titanium Alloys** | | |
| Ti-10V-2Fe-3Al | quasi-static[1] | yes |
| | high rate[2] | yes |
| Ti-8Mn | quasi-static | yes |
| | high rate | yes |
| Ti-6Al-4V | | |
| Commercial | quasi-static | yes[3] |
| | high rate | yes |
| ELI Grade[4] | quasi-static | yes |
| | high rate | yes |
| **Superalloys** | | |
| Alloy 600 | quasi-static | no |
| René 41 | quasi-static | no |
| **Steels** | | |
| HY80 | quasi-static | no |
| | ultra-soft[5] | no |
| | low temperature[6] | no |
| AISI 4340 | quasi-static | yes |
| | ultra-soft | no |
| | high rate | no |
| W1 Tool Steel | quasi-static | no |
| **Aluminum Alloys** | | |
| 7075 | quasi-static | no |
| Al-2w%Cu | quasi-static | no |

1. Quasi-static applied strain rates are typically around $5 \times 10^{-4} s^{-1}$.
2. High strain rate tests were conducted between 10 and $10^4 s^{-1}$.
3. Localized melting could be suppressed in both grades of Ti-6Al-4V by heat treating to a colony $\alpha$ microstructure.
4. Extra Low Interstitial grade (low oxygen and nitrogen content).
5. Large spring strained in series with sample drastically decreasing the stiffness of the test system.
6. Ambient temperature of tests decreased incrementally to ≈-50°C.

(This page intentionally left blank.)

## REFERENCES


1. David D. Makel, Strain Rate Dependent Processes in the Fracture of Ti-8Mn. Doctoral Thesis (Materials Science), University of Virginia, August 1987.

2. J. Daniel Bryant, Deformational Heating at the Crack Tip and Its Role in Fracture of Ti-10V-2Fe-3Al. Ph.D. Thesis, University of Virginia, Jan. 1987.

3. K. Jagannadham, H.-D. Kunze, L. W. Meyer, and H. G. F. Wilsdorf, Proc. ICSMA8, P. O. Kettunen, T. K. Lepistö, and M. E. Lehtonen (Eds.), Pergamon Press, New York, 1988, 1095.

4. A. J. Bedford, A. L. Wingrove and K. R. L. Thompson, J. Aust. Inst. Metals, 19, 61 (1974).

5. K. Jagannadham and H. G. F. Wilsdorf, ZS Metallkd., 80, 628 (1989).

6. D. D. Makel and D. Eylon, Metall. Trans. 21A, 3127 (1990).

7. J. R. Rice and N. Levy, Physics of Strength and Plasticity (A.S. Argon, Ed.) MIT Press (1969) 277.

8. J. M. Krafft and G. R. Irwin, ASTM-STP No. 381, Philadelphia, PA (1965) 114.

9. A. H. Priest, Welding Inst./ASM Int. Conf. on Dynamic Fracture Toughness (1977) 95.

10. K. Jagannadham and M. J. Marcincowski, Unified Theory of Fracture, Trans. Tech. S.A., Switzerland (1983).

11. J. D. Achenbach and M. F. Kanninen, Fracture Mechanics (N. Perrone, H. Liebowitz, D. Mulville, and W. Pilkey, Eds.) Univ. Virginia Press (1978), 649.

12. H. G. Baron, J. Iron and Steel Inst. (London) 182, 354 (1956).

13. F. Seitz and T. A. Read, J. Appl. Phys. 12, 470 (1941).

14. P. Gillis and J. Kelley, Metallurgical Effects at High Strain Rates (R. W. Rhode, B. M. Butcher, J. R. Holland and C. H. Karnes, Eds.) TMS, New York (1973) 287.

15. A. V. Granato, Fundamentals of Deformation and Fracture, IUTAM, Cambridge Univ. Press (1984) 188.

16. J. P. Hirth and J. Lothe, Theory of Dislocations, McGraw Hill, New York (1968).

17. J. Lothe, J. Appl. Phys. 33, 2116 (1962).

18. J. D. Bryant and H. G. F. Wilsdorf, Proc. IMPACT '87, C. Y. Chiem, H.-D. Kunze, and L. W. Meyer (Eds.), D. G. M. Informationsges., Oberursel, Germany, 1988, Vol. 2, 145.

19. K. Jagannadham and H. G. F. Wilsdorf, ONR Technical Report UVA/525425/MS89/104, August 1989.

20. H. G. F. Wilsdorf, Acta Metall. 30, 1247 (1982).

21. H. G. F. Wilsdorf, Nachr. Akademie d. Wissensch. Göttingen, II. Math. Physikal. Kl., 1984, 1.

22. D. D. Makel and H. G. F. Wilsdorf, Impact Loading and Dynamic Behavior of Materials, C. Y. Chiem, H.-D. Kunze, and L. W. Meyers (Eds.), DGM Informationsgesellschaft Verlag, Oberursel, Germany, 1988, Vol. 2, 587.

23. D. D. Makel and H. G. F. Wilsdorf, Scripta Metall., 21, 1229 (1987).

24. H. G. F. Wilsdorf, Mater. Sci. Eng. 59, 1 (1983).

25. H. G. F. Wilsdorf, Fracture, Met. Soc. AIME, W. W. Gerberich and D. L. Davidson (Eds.) Warrendale, PA, 1985, 137.

26. H. G. F. Wilsdorf, ZS Metallkd. 75, 154 (1984).

27. I. M. Robertson, G. M. Bond, H. K. Birnbaum, and H. G. F. Wilsdorf, Fracture, W. W. Gerberich and D. L. Davidson (Eds.) Warrendale, PA, 1985, 119.

28. T. C. Pollock, The Fracture of Beryllium Single Crystals. Ph.D. Thesis, Univ. of Virginia, 1977.

29. K. Jagannadham, T. C. Pollock, and H. G. F. Wilsdorf, Mater. Sci. Eng. A113, 373 (1989).

30. K. Jagannadham and H. G. F. Wilsdorf, Mater. Sci. Eng. 81, 273 (1986).

31. J. D. Bryant, D. D. Makel and H. G. F. Wilsdorf, Mater. Sci. Eng. 77, 85 (1986).

32. Aerospace Structural Metals Handbook, Y. Weiss and J. G. Sessler (Eds ), Vol. I (1963) Syracuse Univ. Press, Code 1206, 6, 7.

33. J. H. Giovanola, in Impact Loading and Dynamic Behavior of Materials, C. Y. Chiem, H.-D. Kunze, and L. W. Meyer (Eds.), D. G. M. Informationsges. Verlag, Oberursel, Germany, 1988, Vol. 2, 705.

34. J. H. Giovanola, Mech. of Mater. 7, 59 (1988).

35. J. H. Giovanola, Mech. of Mater. 7, 73 (1988).

36. F. R. Larson and F. L. Carr, "How Failures Occur...Experiences in the Field," Metal Progress, March 1964, 75.

37. F. R. Larson and F. L. Carr, "How Failures Occur...Topography of Fracture Surfaces," Metal Progress, February 1964, 26.

38. F. L. Carr and Larson, F. R., "Fracture Surface Topography and Toughness of AISI 4340 Steel," Journal of Materials, JMLSA, 4, 865 (1969).

39. Structural Alloys Handbook, Vol. I, 1980 edition, ed. T. D. Moore, Battelle's Columbus Laboratories, Columbus, OH, 4340 Steel section, 70.

40. G. B. Olsen, J. F. Mescall, and M. Azrin, Shock Waves and High-Strain-Rate Phenomena in Metals, Plenum Press, NY (1981) 221.

41. J. H. Holloman, Trans. AIME, 162, 268 (1945).

42. R. von Mises, Göttinger Nachr. Akademie d. Wissensch. Math. Phys. Klasse (1913) 582.

43. P. W. Bridgeman, Trans. Am. Soc. Met., 32, 553 (1944).

44. A. K. Sachedev and J. E. Hunter, Metall. Trans. 13A, 1063 (1982).

45. J. D. Bryant, Micron Micr. Acta 17, 237 (1986).

46. J. D. Bryant and H. G. F. Wilsdorf, Scam. Micro. Suppl. 2, 387 (1988).

47. A. M. Freudenthal and J. H. Weiner, J. Appl. Physics 27, 44 (1956).

## PRESENTATIONS

**Under ONR Contract #N00014-88-K-0111 by the Principal Investigator with graduate students and colleagues**

1. Adiabatic Shear During the Final Separation of Tensile Samples, TMS Annual Meeting, Phoenix, AZ (January 25, 1988), David D. Makel and H. G. F. Wilsdorf.

2. Calculations of the Temperature Rise at Crack Tips During Ductile Fracture, Fraunhofer-Institut/IFAM, Bremen, Federal Republic of Germany (May 17, 1988), H. G. F. Wilsdorf.

3. Modeling Crack Tip Temperatures, Colloquium, Norwegian Technical University, Trondheim, Norway (August 18, 1988), H. G. F. Wilsdorf.

4. The Development of High Temperatures in Titanium Alloys During Fast Fracture, 8th International Conference on the Strength of Metals and Alloys, Tampere, Finland (August 22-26, 1988), K. Jagannadham, N.-D. Kunze, L. W. Meyer and H. G. F. Wilsdorf.

5. Initiation and Propagation of Adiabatic Shear in Tensile Samples, TMS Fall Meeting, Chicago, IL (September 26, 1988), D. D. Makel and H. G. F. Wilsdorf.

6. Modeling the Temperature Rise at the Tip of a Fast Crack, American Physical Society, Raleigh, North Carolina (November 10-12, 1988), K. Jagannadham and H. G. F. Wilsdorf.

7. The Strength and Microstructure of CVD Alpha-Iron Filaments, National Physical Laboratory, New Delhi, India (March 10, 1989), H. G. F. Wilsdorf.

8. The Microstructure of Nano-Crystalline Alpha-Iron, Benares Hindu University, Varanasi, India (March 13, 1989), J. Newkirk and H. G. F. Wilsdorf.

9. Metastable Microstructures in CVD Alpha-Iron, Indo-U.S. Workshop on Metastable Microstructures, Goa, India (April 1, 1989), J. W. Newkirk and H. G. F. Wilsdorf.

10. The Effect of Microstructure on the Formation of Unusual Fracture Surface Features in Ti-6-4 Tensile Samples, TMS Fall Meeting, Indianapolis, Indiana (October 3, 1989), David D. Mekel and D. Eylon.

11. An Investigation of the Formation of Unusual Spheroidized Fracture Surface Features in Steel and Superalloy Tensile Samples, TMS Fall Meeting, Indianapolis, Indiana (October 3, 1989), David D. Makel and H. G. F. Wilsdorf.

12. Localization Melting During the Separation of High Strength Tensile Samples, Explomet 90, La Jolla, California (August 15, 1990), David D. Makel and H. G. F. Wilsdorf.

13. Catastrophic Temperature Increase During the Separation of High Strength Tensile Samples, MFFG45 Conference on Mechanical Failure Prevention, Annapolis, MD (April 9, 1991), David D. Makel and H. G. F. Wilsdorf.

14. The Phenomenon of Localized Melting During the Separation of Tensile Samples, The Fraunhofer-Institut (IFAM), Bremen-Lesum, Germany (July 12, 1991), David D. Makel.

## PUBLICATIONS

Under ONR Contract #N00014-88-K-0111 by the Principal Investigator with graduate students and colleagues

1. "Spatially Varying Crack Tip Stress Fields and Low Energy Dislocation Substructures," International Journal of Fracture, Vol. 34 (1987), pp. 297-307, K. Jagannadham and H. G. F. Wilsdorf.

2. "Investigations of Thermal Effects in Areas of High Shear Caused by Rapid Tensile Separation," Proceedings of IMPACT'87: International Conference on Impact Loading and Dynamic Behaviour of Materials, Eds. Chiem, C. Y., Kunze, H.-D. and Meyer, L. W., pp. 587-594, D. D. Makel and H. G. F. Wilsdorf.

3. "The Effect of Increasing Loading Rate on Tensile Properties and Fracture Toughness of Ti-10V-2Fe-3Al," Proceedings of IMPACT'87: International Conference on Impact Loading and Dynamic Behaviour of Materials, Eds. Chiem, C. Y., Kunze, H.-D. and Meyer, L. W., pp. 145-152, J. D. Bryant and H. G. F. Wilsdorf.

4. "Dislocation Cell Size in a Spatially Varying Stress Field of a Crack Tip Region," Materials Science and Engineering, Vol. A113 (1989), pp. 373-383, K. Jagannadham, T. C. Pollock and H. G. F. Wilsdorf.

5. "Quantifying Fracture Surfaces by Stereo-Photogrammetry," Proceedings of the 6th Pfefferkorn Conference (SEM International, 1988) Ed. O. Johari, pp. 387-393, J. D. Bryant and H. G. F. Wilsdorf.

6. "Dislocation Cell Size in a Spatially Varying Stress Field of a Crack Tip Region," Proceedings, Second International Conference on Low-Energy Dislocation Structures (Charlottesville, Virginia) (August 13-17, 1989) Ed., M. N. Bassim, W. A. Jesser, D. Kuhlmann-Wilsdorf and G. J. Shiflet, pp. 373-383, K. Jagannadham, T. C. Pollock and H. G. F. Wilsdorf.

7. "Modeling the Temperature Rise at the Tip of a Fast Crack," Zeitschrift für Metallkunde, Vol. 80, No. 10 (1989) pp. 698-709, K. Jagannadham and H. G. F. Wilsdorf.

8. "The Effect of Microstructure on Localized Melting at Separation in Ti-6Al-4V Tensile Samples," Metallurgical Transactions, Vol. 21A (December 1990) pp. 3127-3136, D. D. Makel and D. Eylon.

9. "Localized Melting at Separation of AISI 4340 Steel Tensile Samples," Materials Science and Engineering, in press, D. D. Makel and H. G. F. Wilsdorf.

10. "Metastable Microstructures in CVD Alpha-Iron," Proceedings, Indo-U.S. Workshop on Metastable Microstructures, Goa, India (March 30-April 2, 1989), in press, H. G. F. Wilsdorf and J. W. Newkirk.

11. "Localized Melting During the Separation of High Strength Tensile Samples," Applications of Shock-Wave and High-Strain-Rate Phenomena in Materials, Proceedings of the Explomet '90 Conference, La Jolla, California, in press, D. D. Makel and H. G. F. Wilsdorf.

12. "Catastrophic Temperature Increase During the Separation of High Strength Alloys in Tensile Loading," Focus on Mechanical Failures: Mechanisms and Detection, Proceedings of the 45th Meeting of the Mechanical Failures Prevention Group, the Vibration Institute, Willowbrook, IL (1991), pp. 79-88, D. D. Makel and H. G. F. Wilsdorf.

(This page intentionally left blank.)

## DISTRIBUTION LIST

| Copy No. | |
|---|---|
| 1 - 6 | Director<br>Naval Research Laboratory<br>Washington, DC 20375<br>Attention: Code 2627 |
| 7 | Dr. D. E. Polk<br>Program Officer<br>Materials Division<br>Code 1131<br>Office of Naval Research<br>800 N. Quincy Street<br>Washington, DC 22217-5000 |
| 8-19 | Defense Technical Information Center<br>S47031<br>Building 5, Cameron Station<br>Alexandria, VA 22314 |
| 20-21 | H. G. F. Wilsdorf, MS |
| 22-23 | T. H. Courtney, MS |
| 24-25 | Ms. E. H. Pancake, Clark Hall |
| 26-30 | Light Metals Center Office |
| 31-80 | Supplemental Distribution List |
| * | Office of Naval Research Resident Representative<br>818 Connecticut Avenue, N.W.<br>Eighth Floor<br>Washington, DC 20006<br>Attention: Mr. Michael McCracken<br>Administrative Contracting Officer |

*Cover letter